

# Radionuclides as Tracers of Arctic Outflows: Pathways, Water Mass Mixing, and Freshwater input to Davis Strait and the Labrador Sea

Lisa G.T. Leist<sup>1</sup>, Maxi Castrillejo<sup>2</sup>, Kumiko Azetsu-Scott<sup>3</sup>, Craig Lee<sup>4</sup>, Jed Lenetsky<sup>5</sup>, Marc Ringuette<sup>3</sup>, Christof Vockenhuber<sup>1,6</sup>, Habacuc Pérez-Tribouillier<sup>1,6</sup>, Catherine Jeandel<sup>7</sup>, Jean-Éric Tremblay<sup>8</sup>, and Núria Casacuberta<sup>1,6</sup>

<sup>1</sup>Institute of Biogeochemistry and Pollutant Dynamics, Department of Environmental Systems Science, ETH Zurich, Zurich, Switzerland

<sup>2</sup>Institute of Earth Sciences, University of Lausanne, Lausanne, Switzerland

<sup>3</sup>Bedford Institute of Oceanography, Dartmouth, Nova Scotia, Canada

<sup>4</sup>Applied Physics Laboratory, University of Washington, Seattle, Washington

<sup>5</sup>Department of Atmospheric and Oceanic Sciences and Institute of Arctic and Alpine Research, University of Colorado - Boulder, Boulder, Colorado, USA

<sup>6</sup>Laboratory of Ion Beam Physics, Department of Physics, ETH Zurich, Zurich, Switzerland

<sup>7</sup>LEGOS, Université de Toulouse, CNRS, IRD, CNES, UPS, Toulouse, France

<sup>8</sup>Département de biologie, Québec Océan and Takuvik Joint International Laboratory (UMI 3376), Université Laval (Canada)-CNRS (France), Université Laval, Québec, Canada

**Correspondence:** Lisa Leist (lisa.leist@usys.ethz.ch) and Núria Casacuberta (cnuria@ethz.ch)

**Abstract.** In Davis Strait, one of two primary Arctic gateways between the Arctic and Atlantic Oceans, the exchange between northward-flowing Atlantic waters and southward-flowing Arctic waters possibly influences deep-water formation in the subpolar North Atlantic. Yet, these circulation pathways and mixing processes, that may be changing, remain uncertain, underscoring the need for new tracers to resolve their structure and variability. This study employs observations from 2022 and 2024 of two artificial radionuclides, <sup>129</sup>I and <sup>236</sup>U as new tracers of water masses in Baffin Bay, Davis Strait and the Labrador Sea. Samples were collected during three expeditions: the AZOMP occupation of the AR7W Line in May 2022, Davis Strait Observation Program in October 2022, and the Amundsen Expedition as part of the Refuge Arctic and Transforming Climate Action programme in September-October 2024. By defining the characteristic <sup>129</sup>I and <sup>236</sup>U concentrations of the main inflowing waters, we examined the distribution, origin and formation of key water masses in Baffin Bay. Our results reveal a substantial contribution (75%) of West Greenland Shelf Water to Arctic Water on the surface of central Baffin Bay. <sup>236</sup>U-rich Arctic-Atlantic-derived water entering Baffin Bay via Lancaster Sound contributes 40 – 60% to the formation of the Transition Water observed in Baffin Bay. In contrast, cold Arctic Water appears to originate mainly from Nares Strait, and is derived primarily (up to 70%) from Arctic-Atlantic Water. Notably, the contribution of the Baffin Bay Transition Water to the formation of LSW was significant, exceeding 20%. However, the binary mixing model showed limitations in quantifying the origin of North East Atlantic Deep Water due to low tracer concentrations and the likely influence of multiple water mass sources. This study offers novel insights into the origin and transformation of water in Baffin Bay and the Labrador Sea and enhances our understanding of the complex interactions between the Arctic Ocean and the subpolar North Atlantic.

# 1 Introduction

## 1.1 Davis Strait, connecting the Arctic with the subpolar North Atlantic

20 Davis Strait, situated between western Greenland and Baffin Island (Fig. 1A), is a key gateway for the exchange of water masses between the Arctic Ocean and the North Atlantic (Haine et al., 2015; Curry et al., 2014; Huang et al., 2024; Rudels et al., 2004; Komuro and Hasumi, 2005). The sill of Davis Strait, with a depth of approximately 1060 m, defines the southern boundary of Baffin Bay (maximum depth 2300 m) and the northern boundary of the Labrador Sea (maximum depth 3500 m). Through this passage, cold and fresh southward-flowing waters from Baffin Bay meet the northward-flowing warm Atlantic waters entering  
25 from the Labrador Sea. Both the fluxes and the water mass properties in Davis Strait exhibit pronounced seasonal variability (Cuny et al., 2005; Curry et al., 2014). The largest changes in temperature and salinity originate from modifications within Baffin Bay, which receives Arctic-derived waters via the main channels of the Canadian Arctic Archipelago (CAA). These include Nares Strait, connecting to the Eurasian Basin, as well as Lancaster Sound and Jones Sound, which link to the Canada Basin (Münchow et al., 2015; Rudels, 2011; Tang et al., 2004; Pelle et al., 2024). At the same time, Baffin Bay receives an  
30 Atlantic inflow from the Labrador Sea, linking Baffin Bay to the western subpolar gyre and key regions of deep convection, which contribute to the Atlantic Meridional Overturning Circulation (AMOC), the ventilation of deep waters, and the oceanic uptake of anthropogenic CO<sub>2</sub> (Tang et al., 2004; Le Bras, 2023; Lozier, 2023; Rhein et al., 2017).

The exchanges of water masses within Baffin Bay, and their associated variability and impacts, underscore the importance of understanding the complex circulation system of the region. The general circulation in Baffin Bay (Fig. 1A) is largely influenced  
35 by boundary currents. From eastern Davis Strait, the northward-flowing West Greenland Current system (WGC, dark red arrows, Fig. 1A) transports two components along the Greenland shelf. The fresh West Greenland Shelf Water (WGSW, dark red), transported by the West Greenland Coastal Current, and the warm and saline West Greenland Irminger Water (WGIW, light green arrow Fig. 1A), which is confined within a shelf-break jet (Lin et al., 2018; Curry et al., 2014; Huang et al., 2024; Gou et al., 2022). The WGSW originates from the East Greenland Current (EGC, dark red arrow east of Greenland, Fig. 1A),  
40 which outflows Fram Strait and flows south along the Greenland shelfbreak, carrying fresh and relatively warm Polar Surface Water (PSW) from the Arctic Ocean (Sutherland et al., 2009). After rounding the southern tip of Greenland at Cape Farewell, the EGC is joined by WGIW at depth. The warm and saline WGIW originates from the North Atlantic Current (NAC, black arrows Fig. 1A), carrying water from the subtropics (Cuny et al., 2002). Towards the northern Labrador Sea, the current system of west Greenland becomes baroclinically and barotropically unstable due to the steep continental slope, leading to large  
45 anticyclonic eddies. The eddies are known as Irminger Rings and carry both the WGSW and WGIW offshore into the Labrador Sea (Chanut et al., 2008; Zou et al., 2024; Gelderloos et al., 2011). In the northern Labrador Sea, the WGC bifurcates into two branches, with one continuing north into Baffin Bay, and a larger branch following the bathymetry of the Labrador Sea, turning westward towards the Labrador Shelf (Myers et al., 2009; Huang et al., 2024; Gou et al., 2022).

Western Davis Strait is dominated by the southward-flowing surface Baffin Island Current (BIC, orange arrow Fig. 1A),  
50 which transports fresh water of Arctic origin, such as Arctic Water (AW) and cold Arctic Water (cold AW), along the Baffin Island shelf and slope to the Labrador Sea (Cuny et al., 2005). While Arctic Water is strongly influenced by glacial run-off and

sea ice melt (Curry et al., 2014; Azetsu-Scott et al., 2012), cold Arctic Water (similar to the hydrographic properties of cold Polar Water; Huang et al. (2024)) represents a subset of cold and more saline water within Arctic Water, which experienced winter convection by stronger cooling and salinification (Shan et al., 2024). Waters exiting the Arctic Ocean enter Baffin Bay through the shallow sills of Nares Strait (220 m, Jackson et al., 2014; Rabe et al., 2010), Lancaster Sound (125 m, Peterson et al., 2012) and Jones Sound (125 m, Melling et al., 2008; Pelle et al., 2024). These water masses with low salinities (<33.5) and low temperatures (<1°C) are present primarily at the surface of Baffin Bay and along the BIC.

In central Davis Strait, at intermediate depths between 300 m and 600 m, relatively warm Transition Water (dark blue Fig. 1A) flows throughout the year and at low velocities out of Baffin Bay (Huang et al., 2024; Curry et al., 2014). Rudels (2011) described Transition Water as an intermediate layer formed by mixing Atlantic water from the south and colder water from the north. More recently, Huang et al. (2024) identified two different types of Transition Water, each resulting from the mixing of several water masses. Further, Lehmann et al. (2022) identified a temperature maximum in western Baffin Bay aligning with the warmest and deepest fraction of Transition Water. Below Transition Water, down to 1600 m depth, the water column is dominated by Baffin Bay Mode Water (BBMW), also known as Baffin Bay Deep Water, whose formation processes remain unclear (Lehmann et al., 2019; Bourke et al., 1989). In central Baffin Bay, depths greater than 1600 m are filled by old Baffin Bay Bottom Water (BBBW) (Bourke et al., 1989), which is not observed in the Davis Strait outflow (Curry et al., 2014).

South of Davis Strait, the cold, fresh surface water from the BIC joins the Labrador Current, where they mix with cool, fresh outflow from the Hudson Strait and water from the WGC that turned westward, bathymetrically steered at the Labrador Sea (García-Ibáñez et al., 2015; Cuny et al., 2002; Myers, 2005; Straneo and Saucier, 2008).

In the Labrador Sea, the Irminger Rings detach from the boundary current and drift into the central basin. This water contributes to the formation of Labrador Sea Water (LSW, light blue arrows in Fig. 1A), together with fresh water from the Labrador Current, which accounts for approximately 6-8% of LSW (Myers, 2005; Lilly et al., 2003; Hátún et al., 2007). The annual deep winter convection that forms the LSW represents a key component of the AMOC (Yashayaev, 2007; Bower et al., 2009; Lavelander et al., 2005). Other water masses in the Labrador Sea include the North East Atlantic Deep Water (NEADW, yellow arrow in Fig. 1A), which follows the cyclonic Deep Western Boundary Current and is found below LSW at approximately 2000 m depth. The NEADW forms by mixing of multiple source water inflows from east of Greenland, including LSW, Denmark Strait Overflow Water (DSOW, dark green in Fig. 1A), and Iceland Scotland Overflow Water (ISOW, light green in Fig. 1A) (Yashayaev, 2007; Tanhua, 2005; Dickson and Brown, 1994; García-Ibáñez et al., 2015). The bottom depths are occupied by DSOW and carried primarily by the Deep Western Boundary Current from its formation region in the Nordic Seas towards the Grand Banks (Dale et al., 2024; Leist et al., 2024; Rudels, 2011).

Decades of oceanographic studies have significantly improved our understanding of water mass composition and volumetric transport in Davis Strait, Baffin Bay, and the Labrador Sea (Bourke et al., 1989; Yashayaev, 2007; Curry et al., 2011). However, climate-driven changes are altering the circulation and freshwater dynamics of the region (Shan et al., 2024). Under climate change, the Arctic is warming at nearly four times the global average, yet current ocean models appear to under-represent this rapid evolution (Rantanen et al., 2022). Observational evidence shows that weakened stratification in the Eurasian Basin of

the Arctic Ocean is driving structural changes in the water column—a process known as "Atlantification". This shift enables warm Atlantic water to penetrate further north, accelerating sea ice melt and reducing winter sea ice formation (Polyakov et al., 2025, 2017; Wang et al., 2024). Historically, approximately half of the exported Arctic freshwater has been exported through the CAA and into Baffin Bay (Haine et al., 2015). In recent years, increased glacial melt from Greenland and the CAA (The IMBIE Team, 2020; Vandecrux et al., 2024; Gardner et al., 2011) has led to more frequent ice-free channels during summer (Canadian Ice Service; <http://ice-glaces.ec.gc.ca/>), likely modifying freshwater exchange between the Arctic and Baffin Bay (Malles et al., 2025). Furthermore, Baffin Bay now receives increasing volumes of glacier meltwater from Greenland, a trend accelerated by the warming influence of Atlantic water (Holland et al., 2008; Bamber et al., 2018).

95 The established pathways of water mass exchange between high latitudes and the subpolar North Atlantic may also be changing (Weijer et al., 2022; Carmack et al., 2016). Freshwater discharge (water with practical salinity below 34.6, Zhang et al. (2021a)) from Davis Strait into the subpolar North Atlantic is projected to increase, potentially affecting deep convection in the Labrador Sea (Zhang et al., 2021b; Wang et al., 2023; Yashayaev, 2024; Zhang et al., 2021a). Despite Davis Strait's role as a freshwater source to the subpolar North Atlantic (Shan et al., 2024; Azetsu-Scott et al., 2012; Huang et al., 2024), the freshwater dynamics of both Davis Strait and Baffin Bay remain poorly constrained. This is largely due to strong seasonal variability in freshwater release and the limited access during winter imposed by sea ice cover (Curry et al., 2014; Haine et al., 2015).

100 Additionally, the contribution of water outflowing Davis Strait on the water mass formation in the Labrador Sea remains uncertain. This is likely due to intense winter convection in the Labrador Sea, which strongly modifies temperature and salinity, complicating efforts to trace the origins of water using only these properties (Rudels, 2011; Yashayaev, 2007; Clarke and Gascard, 1983).

105 Furthermore, the role of Baffin Bay intermediate and deep water (e.g. Transition Water) in the formation of LSW remains poorly understood compared to the better-known origin and pathways of surface water (Curry et al., 2014; Cuny et al., 2005). Also, recent studies have emphasised the importance of Arctic freshwater export to the subpolar North Atlantic (Malles et al., 2025; Duyck et al., 2025; Myers, 2005) and the role of cross-density lateral mixing in the Labrador Sea, contributing approximately 60% to the annual formation of LSW (Zou et al., 2023; Pickart and Spall, 2007). However, most observational studies continue to focus on boundary current systems, leaving off-boundary water exchanges understudied (Huang et al., 2024; Curry et al., 2011; Azetsu-Scott et al., 2012). Therefore, a better understanding of the off-shelf and intermediate circulation between Baffin Bay and the Labrador Sea is still needed (Rudels et al., 2004), particularly regarding the origin and formation of Transition Water in Baffin Bay and the potential contributions of Arctic origin freshwater to the formation of LSW.

## 115 **1.2 Using radionuclides to trace water mass origin**

To advance on these complex water-mass interactions, we propose a novel approach in the region that combines the two long-lived artificial radionuclides  $^{129}\text{I}$  ( $t_{1/2}=15.7$  Ma) and  $^{236}\text{U}$  ( $t_{1/2}=23.4$  Ma), with hydrographic properties such as salinity and temperature. We expect  $^{129}\text{I}$  and  $^{236}\text{U}$  to suitably trace circulation patterns and mixing in the Davis Strait region because in-flowing water presents contrasting tracer concentrations measured for the Pacific, Atlantic and Arctic oceans (Wefing et al., 120 2021; Payne et al., 2024; Leist et al., 2024; Castrillejo et al., 2018; Dale et al., 2024).

$^{129}\text{I}$  and  $^{236}\text{U}$  originate primarily from nuclear sources and are assumed to be conservative in seawater (Christl et al., 2015; Casacuberta and Smith, 2023). Their input into the ocean was dominated by a peak in  $^{236}\text{U}$  from the nuclear weapons test global fallout in the 1960s, and liquid releases from nuclear fuel reprocessing plants in Sellafield (UK) and La Hague (France) (Fig. 1A, black factory symbols), peaking in the 1980s for  $^{236}\text{U}$  and ramping up after 1990s for  $^{129}\text{I}$ . Fig. A1 represents their  
125 input function defined at 70°N (blue star in Fig. 1A), a combination of global fallout and liquid releases from the nuclear reprocessing plants (Wefing et al., 2021; Payne et al., 2024). In both cases, the released radionuclides flow north from the North Sea and join the Norwegian Coastal Current (NCC), entering the Arctic Ocean. From the entrance of the Arctic Ocean, the radionuclides can recirculate within the Eurasian Basin in a short loop or a longer path (Canada Basin) before exiting the Arctic Ocean via Fram Strait or the CAA (Li et al., 2020; Rudels et al., 1994; Payne et al., 2024; Casacuberta and Smith, 2023). From  
130 Fram Strait, the radionuclides are transported south and ultimately reach the Labrador Sea and Baffin Bay as part of the WGC (Wefing et al., 2019; Dale et al., 2024; Leist et al., 2024). Up to date, there are no measurements of these two tracers in either Nares Strait or the CAA, so their transport through these routes is still unknown.

In the Arctic Ocean, the transport times and mixing of Atlantic Water can be calculated using different models that are all based on tracer input functions (Fig. A1) (Wefing et al., 2021; Payne et al., 2024). However, in sub-Arctic regions, the simultaneous  
135 mixing of multiple water masses with distinct input functions complicates the accurate estimation of water age and mixing when relying solely on these tracers. Nevertheless, the combination of  $^{129}\text{I}$  and  $^{236}\text{U}$  has already proven to be a suitable tool to study the formation and origin of water masses in the subpolar North Atlantic, where it can be assumed that both tracers are in a steady state for each water mass (Castrillejo et al., 2018; Leist et al., 2024; Dale et al., 2024).

In the study area, we expected to find a wide representation of the historical temporal variation of the tracers, allowing us  
140 to disentangle the origin of Atlantic water. While the "old" Arctic-Atlantic Water (AAW) from the Canada Basin would be characterised by high  $^{236}\text{U}$  and low  $^{129}\text{I}$  (Payne et al., 2024), the "young" Polar Surface Water (PSW) recirculated in the Eurasian Basin would carry a higher signal of  $^{129}\text{I}$  (Wefing et al., 2025). Low tracer concentrations should be characteristic of the WGIW, which enters the study region from the subtropics without direct contact with the radionuclides (Castrillejo et al., 2018; Dale et al., 2024; Leist et al., 2024). Also, Pacific Water (salinity of 32.5) entering Baffin Bay through the CAA  
145 would carry low concentrations of both radionuclides, as their only source was the atmospheric weapon tests (Payne et al., 2024). Finally, it is important to note that the freshest water (i.e. glacier melt, sea ice melt, and river run-off: Shadwick et al. (2011); Grenier et al. (2022); Bamber et al. (2018); Malles et al. (2025)) should contain almost no tracer, hereinafter denoted as tracer-free water (Casacuberta et al., 2016).

150 In this study, we address critical knowledge gaps in understanding water mass transformations and exchanges between Baffin Bay, Davis Strait and the Labrador Sea by applying a novel approach based on the two long-lived artificial radionuclides,  $^{129}\text{I}$  and  $^{236}\text{U}$ . The tracers, which exhibit distinct distributions across Arctic and Atlantic origin water, offer a complementary tool to traditional hydrographic parameters such as temperature and salinity, enabling the identification of water mass sources in regions characterised by complex mixing and strong seasonal variability. Using observations collected between 2022 and 2024  
155 across key Arctic gateways—including Davis Strait, Nares Strait, Lancaster Sound—and the Labrador Sea, we apply a binary

mixing model to characterise tracer signatures of inflowing water masses and quantify their contributions to key intermediate and deep water masses. This approach allows us to explore the origin of the Transition Water, BBMW, BBBW and (cold) Arctic Water and to follow the evolution of WGSW and WGIW along their cyclonic journey through the Baffin Bay. It also enables us to assess the potential influence of Transition Water on water mass formation in the Labrador Sea.

## 160 2 Methods

### 2.1 Sample collection and processing

Seawater samples were collected from multiple sites (Fig. 1B). In May 2022, along the AR7W Line across the Labrador Sea, seawater was collected from the surface and six depth profiles (depth range: surface - 3560 m), including four surface samples from southwest of the AR7W Line, aboard R/V Atlantis as a part of the Atlantic Zone Off-Shelf Monitoring Program (AZOMP) 165 by Bedford Institute of Oceanography (red triangles). In October 2022, additional sampling was conducted in the Davis Strait region aboard R/V Neil Armstrong as part of Davis Strait Observing System Program. This survey included a depth profile in central Baffin Bay (Fig. 1B, red square, depth range: surface - 2377 m), and full transects along the Northern Line (9 stations, Fig. 1B red circles, depth range: surface - 1665 m), Davis Strait (10 stations, red diamonds Fig. 1B, depth range: surface - 1013 m) and Northern Labrador Sea Line (9 stations, Fig. 1B red stars, depth range: surface - 2614 m). Further sampling was 170 conducted in September-October 2024 during the Refuge Arctic Cruise Legs 4 and Transforming Climate Action Leg 5, both onboard CCGS Amundsen, targeting Nares Strait and Lancaster Sound. In northern Nares Strait, two stations were sampled: one depth profile (50-345 m, RA28) and one surface station (RA34). Both are represented in Fig. 1B as one unfilled orange square. In the southern Nares Strait, three stations were sampled: RA44, RA48, RA50, of which only RA48 is a depth profile (70-600 m). These stations are represented in Fig. 1B as unfilled orange circles. In Lancaster Sound, two sites were sampled 175 in the western part of the Archipelago (Keb/TCA-S3, depth range: 2-140 m, unfilled red triangles in Fig. 1B), and the eastern part close to Baffin Bay (TCA S3, depth range: 2-890 m, unfilled red diamond in Fig. 1B). All cruises used a CTD-Rosette equipped with 24-12 L Niskin bottles to collect samples for the purpose of this study.

Seawater samples for  $^{129}\text{I}$  analysis were collected in 250 ml brown plastic bottles, and pre-rinsed three times with water from the Niskin bottle, before being filled. For  $^{236}\text{U}$ , 2-3 L of seawater were collected in Nalgene cubitainers, also pre-rinsed 180 three times before filling them. All samples were stored onboard without any further processing, sent to ETH Zurich for the analysis of iodine and uranium isotopes.

The radiochemistry of  $^{129}\text{I}$  and  $^{236}\text{U}$  was performed following Wefing et al. (2019) and Leist et al. (2024) for a total of 307 samples. The samples were analysed using the TANDY AMS system at the Laboratory of Ion Beam Physics (LIP), ETH Zurich (Vockenhuber et al., 2015). The  $^{129}\text{I}$  concentrations were calculated using the measured  $^{127}\text{I}/^{129}\text{I}$  atom ratio and the 185 known amount of spiked  $^{127}\text{I}$ . The reproducibility of  $^{129}\text{I}$  data was estimated based on repeated measurements of an internal seawater standard ( $n=14$ , average  $^{129}\text{I}= 10.4\pm 0.5\times 10^7$  at/kg). Blanks for  $^{129}\text{I}$  ( $n=16$ ,  $7.6\pm 1.5\times 10^5$  at) were obtained using deionised water treated following the same procedure as for seawater samples.

The samples for  $^{236}\text{U}$  were spiked with 1 pg of  $^{233}\text{U}$  following the radiochemistry described by Wefing et al. (2021) and

Leist et al. (2024). The MILEA AMS system at LIP facility (Christl et al., 2013, 2023) was used to measure  $^{233}\text{U}/^{238}\text{U}$  and  $^{236}\text{U}/^{238}\text{U}$  in the samples and the in-house standard "ZUTRI". Correction procedures were applied as described by Christl et al. (2023). The concentrations of  $^{236}\text{U}$  and  $^{238}\text{U}$  were calculated based on the known amount of  $^{233}\text{U}$  that was spiked in the sample. Each batch included one blank ( $n=11$ ,  $^{236}\text{U}$ :  $0.01 \pm 0.01 \times 10^6$  at), consisting of deionised water that was treated like the samples.

The results of  $^{129}\text{I}$  and  $^{236}\text{U}$  are reported and plotted in atoms per kg of seawater (at/kg). The combined uncertainty of chemical processing and measurements for both  $^{129}\text{I}$  and  $^{236}\text{U}$  was below 6%. All results and detailed analytical uncertainties are reported in the Zenodo database (<https://doi.org/10.5281/zenodo.16914587>).

## 2.2 Water mass classification

The water masses are summarised in Table A1, and were assigned according to previous water mass classifications in the literature (Curry et al., 2014; Huang et al., 2024; García-Ibáñez et al., 2015; Bourke et al., 1989; Lehmann et al., 2022) and identified using conservative temperature (CT) and absolute salinity ( $S_A$ , see T-S diagram in Fig. A2). The conversion from practical to absolute salinity and from potential to conservative temperature was performed according to TEOS-10 (IOC and IAPSO, 2010). Temperature and salinity are also represented along sections in Fig. A3 to facilitate the comprehensive distribution of water masses. West Greenland Irminger Water (WGIW;  $\text{CT} > 3.5^\circ\text{C}$ ,  $S_A > 34.7$ ) is the warmest and most saline water mass, confined to intermediate depths along the Greenland shelf. West Greenland Shelf Water (WGSW;  $\text{CT} < 5^\circ\text{C}$ ,  $S_A < 34.2$ ) is fresher than WGIW and located at the surface along the Greenland shelf. Arctic Water (AW;  $\text{CT}$ :  $-0.8 - 1.1^\circ\text{C}$ ,  $S_A > 32.9$ ) is the freshest water mass, confined to the Baffin Island and Canadian shelf. The CT and  $S_A$  ranges used here differ significantly from those in Curry et al. (2014); we applied a narrower range for Arctic Water and distinguished it from cold Arctic Water (cold AW;  $\text{CT} < -0.8^\circ\text{C}$ ,  $32.5 < S_A < 33.8$ ), which is colder and more saline. Below the cold Arctic Water, Transition Water ( $\text{CT} < 1.8$ ,  $S_A$ : 34-34.6) is characteristic of mid-depth in Baffin Bay and Davis Strait. Within Transition Water, temperature increases with depth to a temperature maximum ( $\text{CT}$ :  $1.4 - 1.8^\circ\text{C}$ ,  $S_A = 34.64 \pm 0.03$ , Lehmann et al. (2022)). In Baffin Bay, at depths of 600 – 1000 m, Baffin Bay Mode Water (BBMW;  $\text{CT}$ :  $0.7 - 1.2^\circ\text{C}$ ,  $S_A = 34.6$ ; Huang et al. (2024)) was observed overlying Baffin Bay Bottom Water (BBBW;  $\text{CT} < 0.4^\circ\text{C}$ ,  $S_A = 34.6$ ; Bourke et al. (1989), Fig. A3). In the Labrador Sea, Labrador Sea Water (LSW;  $\text{CT}$ :  $3.1 - 3.8^\circ\text{C}$ ,  $S_A > 35.0$ ; García-Ibáñez et al. (2018)) resides at intermediate depth. Beneath LSW, North East Atlantic Deep Water (NEADW;  $\text{CT}$ :  $2.0 - 3.3^\circ\text{C}$ ,  $S_A = 35.07 \pm 0.2$ ; Yashayaev (2007)) overlies Denmark Strait Overflow Water (DSOW;  $\text{CT} < 1.3^\circ\text{C}$ ,  $S_A = 35.0 \pm 0.1$ ; García-Ibáñez et al. (2018)). In Nares Strait and Lancaster Sound, water masses were classified as Arctic Water CAA ( $\text{AW}_{CAA}$ ;  $\text{CT} < 0^\circ\text{C}$ ,  $S_A < 33$ ) and Arctic Atlantic Water CAA ( $\text{AAW}_{CAA}$ ;  $\text{CT} > -1^\circ\text{C}$ ,  $S_A > 33$ ). Samples that do not fall within the defined water mass categories are considered mixtures of the above water types. While all samples are presented in the results section, the discussion focuses on those assigned to specific water masses.

## 220 2.3 Binary Mixing Model

In the study area, several potential water masses are adjacent to those observed in Baffin Bay. These include tracer-free water, Pacific Water (Azetsu-Scott et al., 2012), WGIW (Curry et al., 2014), WGSW (Curry et al., 2014), Polar Surface Water from the Eurasian Basin (Münchow et al., 2006; Wefing et al., 2025), and Arctic-Atlantic Water originating from the Canada Basin (Lehmann et al., 2022; Payne et al., 2024). Further assessment of their formation processes will be based on the conservative tracer signatures of  $^{129}\text{I}$  and  $^{236}\text{U}$ . However, the number of water masses considered exceeds the number of available conservative tracers. Therefore, the complexity of the model is reduced by modelling the mixing fractions of samples between the two most dominant water mass sources (hereinafter referred as endmembers), instead of employing an Optimum Multiparameter Analysis. Before quantifying the origin and estimating the mixing fractions, the water masses are classified according to their temperature and salinity. Then, a binary mixing model combining both  $^{236}\text{U}$  and  $^{129}\text{I}$  is used, as previously described by Leist et al. (2024) and Dale et al. (2024). The water masses in the study area are considered as conservative mixtures of different endmembers. The endmembers are source components of a mixture and set the boundaries of the mixing model. In this study, each endmember has a distinct and characteristic value for temperature, salinity, and  $^{129}\text{I}$  and  $^{236}\text{U}$  concentrations (see details on each endmember in Section 4.1).

In most cases, the  $^{129}\text{I}$  and  $^{236}\text{U}$  concentrations of the endmember consist of an average concentration of several samples collected in this and previous studies, with an associated uncertainty that corresponds to the standard deviation of the average values (see Table A2). Considering the two endmembers as the primary water-mass sources, the resulting water mass is treated as a mixture of the two. The mixing fraction  $f$  is then estimated as:

$$f = \frac{\|\vec{a}\|}{\|\vec{b}\|} \quad (1)$$

where  $\vec{b}$  is the vector connecting the two endmembers (mixing line), and  $\vec{a}$  is the vector connecting a given sample to one of the endmembers. The resulting value of  $f$  represents the percentage contribution of each endmember to a given watermass. This study focuses on different contributions of Atlantic-derived water, and not on the differentiation between different freshwater sources, which are more precisely addressed using nutrients and  $\delta^{18}\text{O}$  (Azetsu-Scott et al., 2012). A key limitation of this model is the assumption that mixing occurs exclusively between two endmembers. If a sample falls outside the defined mixing line, its composition is estimated by projecting orthogonally onto the mixing line and neglecting potential contributions from a third endmember. The model also assumes a steady state for transient tracers, which was previously discussed and justified by Leist et al. (2024) and Dale et al. (2024). In the study region, changes in water mass formation and mixing ratios between endmembers are believed to have a greater influence on tracer concentrations than recent changes in the tracer input function (Fig. A1), supporting the steady-state assumption. The resulting mixing fractions will only be discussed in Section 4 (not in results) and summarised in Table A3.

This section presents individual depth profiles from Nares Strait and Lancaster Sound (Fig. 2), followed by a description of the distribution along the three transects from southern Baffin Bay (Northern Line), Davis Strait, to northern and southern Labrador Sea (Northern Labrador Sea and AR7W lines). To better reflect the general distribution patterns, each water mass is described across the lines/panels (Fig. 3) as a whole, rather than within individual sections. In the sections below, note that  $S_A$  stands for Absolute Salinity, and CT for Conservative Temperature. Details about tracer concentrations, uncertainties, and hydrographic properties are provided in the Zenodo database (<https://doi.org/10.5281/zenodo.16914587>) and the abbreviations for water masses can be found in the Appendix Table A1.

### 3.1 $^{129}\text{I}$ and $^{236}\text{U}$ in Nares Strait and Lancaster Sound

Depth profiles collected in Nares Strait are represented in Fig. 2A and B as orange symbols. Both tracers show low concentrations at the surface Arctic Water (AW,  $^{129}\text{I}$ :  $60\text{--}85 \times 10^7$  at/kg,  $^{236}\text{U}$ :  $11\text{--}14 \times 10^6$  at/kg) and a local maximum in the Arctic Atlantic Water at about 250 m (AAW,  $^{129}\text{I}$ :  $180\text{--}210 \times 10^7$  at/kg,  $^{236}\text{U}$ :  $23 \times 10^6$  at/kg). Below that depth,  $^{129}\text{I}$  seems to slightly decrease towards the bottom, while  $^{236}\text{U}$  remains more constant. Furthermore, the concentrations of both isotopes appear to be higher in the northern part of Nares Strait (squares) compared to the south (circles).

The two profiles in Lancaster Sound are represented in Fig. 2A and B as red symbols. Similar to Nares Strait, the highest concentrations of  $^{129}\text{I}$  were associated with AAW<sub>CB</sub> (Canada Basin) located at 200 m in eastern Lancaster Sound ( $^{129}\text{I}$ :  $130 \times 10^7$  at/kg,  $S_A$ : 33.85, CT:  $-0.10$  °C) and at depths below 140 m in the western station ( $^{129}\text{I}$ :  $120 \times 10^7$  at/kg,  $S_A$ : 33.6, CT:  $-0.44$  °C). In western Lancaster Sound, the highest concentration of  $^{236}\text{U}$  was observed at 10 m depth in Arctic Water ( $^{236}\text{U}$ :  $19 \times 10^6$  at/kg,  $S_A$ : 30.58, CT:  $-0.04$  °C), and the lowest at the surface ( $^{236}\text{U}$ :  $15 \times 10^6$  at/kg). A similar distribution was observed in the eastern Lancaster Sound, with the lowest concentration at the surface ( $^{236}\text{U}$ :  $13 \times 10^6$  at/kg), and a maximum at 200 m ( $^{236}\text{U}$ :  $22 \times 10^6$  at/kg), which then decreased slightly with increasing depth to  $15 \times 10^6$  at/kg at 886 m.

### 3.2 $^{129}\text{I}$ and $^{236}\text{U}$ in central and southern Baffin Bay, Davis Strait and the Labrador Sea

Along all transects (Fig. 3), the highest  $^{129}\text{I}$  concentrations were observed in West Greenland Shelf Water (WGSW), at the surface of the Greenland shelf (Fig. 3A-D). The concentrations of  $^{129}\text{I}$  decreased along the pathway of the West Greenland Current (WGC), with WGSW dropping from  $320 \times 10^7$  at/kg at AR7W in the Labrador Sea (Fig. 3D) to  $170 \times 10^7$  at/kg at the Northern Line in Baffin Bay (Fig. 3A). In contrast, the warmest and most saline West Greenland Irminger Water (WGIW) generally showed increasing  $^{129}\text{I}$  concentrations from  $50 \times 10^7$  at/kg at AR7W to a maximum of  $90 \times 10^7$  at/kg at the Northern Line. In Arctic Water, the freshest water along the Baffin Island Current (BIC) and Labrador Current (LC),  $^{129}\text{I}$  concentrations increased slightly from central Baffin Bay ( $140 \times 10^7$  at/kg, blue squares Fig. 2C) to the Northern Labrador Sea Line ( $150 \times 10^7$  at/kg, Fig. 3C). But, Arctic Water showed lower concentrations ( $100 \times 10^7$  at/kg) at the AR7W Line in the southern Labrador Sea. Cold Arctic Water exhibited elevated  $^{129}\text{I}$  concentrations in the  $100 - 170 \times 10^7$  at/kg range and showed no clear north-south trend. While Arctic Water, WGIW and WGSW were present in all sections, Transition Water was only present along the

Northern Line, Davis Strait (Fig. 3A, B) and central Baffin Bay (Fig. 2C, blue squares), with concentrations in the range of  $50 - 120 \times 10^7$  at/kg, respectively. BMW was observed along the Northern Line, Davis Strait and central Baffin Bay only, with  $^{129}\text{I}$  concentrations of  $29 - 37 \times 10^7$  at/kg.  $^{129}\text{I}$  concentrations at the levels of the blanks ( $<1.2 \pm 1.5 \times 10^7$  at/kg) were measured in  
285 BBBW present below 1600 m in central Baffin Bay and the Northern Line. Labrador Sea Water (LSW) and North East Atlantic Deep Water (NEADW) (only sampled at AR7W, Fig. 3D) covered an  $^{129}\text{I}$  range of  $30-70 \times 10^7$  at/kg at intermediate depth in the Labrador Sea, while the near-bottom Denmark Strait Overflow Water (DSOW) presented concentrations up to  $120 \times 10^7$  at/kg.

The distribution of  $^{236}\text{U}$  concentrations (Fig. 3E – H) differs from that of  $^{129}\text{I}$ . The highest  $^{236}\text{U}$  was observed in the Transition  
290 Water (Fig. 3E, F), with up to  $19 \times 10^6$  at/kg in central Baffin Bay (Fig. 2D, blue squares), followed by cold Arctic Water, with  $^{236}\text{U}$  in the  $14-17 \times 10^6$  at/kg range between Davis Strait (Fig. 3F) and central Baffin Bay. While the  $^{236}\text{U}$  concentration in Arctic Water was generally in the range of  $13 - 15 \times 10^6$  at/kg, the AR7W Line recorded the maximum value ( $16 \times 10^6$  at/kg, Fig. 3H). In water inflowing Davis Strait, such as WGSW,  $^{236}\text{U}$  concentrations decreased slightly towards the north, from  $15 \times 10^6$  at/kg at the AR7W Line to  $13 \times 10^6$  at/kg at the Northern Line (Fig. 3E). Similarly to  $^{129}\text{I}$ , low  $^{236}\text{U}$  concentrations  
295 were measured in WGIW, with an increasing trend from  $9 \times 10^6$  at/kg at AR7W to  $11 \times 10^6$  at/kg on the Northern Line.

In the Labrador Sea, LSW presented  $^{236}\text{U}$  concentrations on the  $9-11 \times 10^6$  at/kg range on the AR7W and Northern Labrador Sea lines (Fig. 3G, H). NEADW, only sampled along AR7W, showed  $^{236}\text{U}$  concentrations slightly above LSW ( $10-12 \times 10^6$  at/kg). The sampling density of DSOW was smaller in the Northern Labrador Sea Line than for AR7W and confined at slightly lower concentrations (AR7W:  $12-14 \times 10^6$  at/kg, Northern Labrador Sea Line:  $12 \times 10^6$  at/kg). Moving towards the Baffin  
300 Bay, the BMW had similar  $^{236}\text{U}$  concentrations of  $10-12 \times 10^6$  at/kg. Finally, in BBBW occupying depths below 1600 m in central Baffin Bay (blue squares Fig. 2D) and the Northern Line,  $^{236}\text{U}$  concentrations reached the analytical limit of detection ( $1.2 \pm 1.5 \times 10^6$  at/kg).

Both tracers have concentrations well above global fallout, which would be about  $2.2 \times 10^7$  at/kg for  $^{129}\text{I}$  and  $5.4 \times 10^6$  at/kg for  $^{236}\text{U}$ , according to recent estimates at the Bering Strait (Payne, 2026). Only the bottom water at Baffin Bay (BBBW)  
305 presents tracer concentrations lower than expected from the global fallout.

### 3.3 Water masses in T – S and $^{129}\text{I} - ^{236}\text{U}$ tracer space

Figure 4 provides an overview of the water masses observed in Baffin Bay, Davis Strait and the Labrador Sea and their distribution in T – S diagram (Fig. 4A) and  $^{129}\text{I} - ^{236}\text{U}$  tracer space (Fig. 4B) while the sampling location is indicated by the symbols and can be referred to in Fig. 1B.

310 WGSW (dark-red symbols) stands out in both panels due to its relatively high temperature and low salinity (Fig. 4A), as well as its elevated  $^{129}\text{I}$  concentrations (from 180 to  $>300 \times 10^7$  at/kg) (Fig. 4B). Its seasonal variability in temperature (Fig. 4A) is consistent with observations by Curry et al. (2014) and Zweng and Münchow (2006) and clearly expressed in the broad temperature range with  $\text{CT} < 0$  °C along the AR7W Line (dark red triangles) sampled in spring and  $\text{CT} > 2$  °C at the other sections sampled in autumn. In the tracer space, WGSW forms a well-defined linear relationship, despite the seasonality.  
315 This indicates that the tracers are largely insensitive to seasonal changes. The saline and warm WGIW (Fig. 4A, light green

symbols) is located at the lower left in tracer space (Fig. 4B, light green symbols) due to its low  $^{129}\text{I}$  and  $^{236}\text{U}$  concentrations. Radionuclide tracers are especially low for samples collected in the Labrador Sea, then they increase slightly together with a freshening and cooling experienced on the northward flow of WGIW.

Arctic Water (Fig. 4, light brown symbols) is fresh and cold and shows tracer concentration slightly below cold Arctic Water (Fig. 4, teal symbols), which is characterised by its distinct temperature minimum and confined to the upper 100 m. Both water masses are positioned in the tracer space at the mixing interface between the relatively warm Transition Water and WGSW.

Within the Transition Water (light blue symbols), the samples located at the temperature maximum ( $\text{TrW}_{\text{Tmax}}$ , dark-blue symbols) exhibit the highest  $^{236}\text{U}$  concentrations. This  $\text{TrW}_{\text{Tmax}}$  lies between cold Arctic Water (teal symbols) and WGIW (light green symbols) in T–S space, consistent with its intermediate hydrographic character (Fig. 4A). In tracer space, however, the  $\text{TrW}_{\text{Tmax}}$  shows the highest  $^{236}\text{U}$  levels within the region (Fig. 4B), second only to the concentrations observed in Nares Strait (orange symbols) and Lancaster Sound (red symbols).

At depth below Transition Water and low temperatures is the BMW (light purple squares and circles) confined at low  $^{129}\text{I}$  and intermediate  $^{236}\text{U}$  concentrations, leading to the even deeper and colder BBBW (purple squares and circles). The BBBW in the Northern Line and central Baffin Bay is found in the bottom left corner of the tracer space and its concentrations of  $^{129}\text{I}$  and  $^{236}\text{U}$  approach the analytical limit of detection.

In the Labrador Sea, surface water (light red symbols) fills the gap tracer between WGSW and WGIW and bridges WGSW and LSW (blue triangles) in the T – S diagram. LSW is colder than WGIW but warmer than the deeper NEADW (yellow triangles). In the tracer space, both LSW and NEADW are located close to WGIW but shifted towards slightly higher  $^{236}\text{U}$  concentrations.

Finally, DSOW (Fig. 4, green symbols), is characterised by low temperatures, high salinity, and intermediate tracer concentrations.

## 4 Discussion

To investigate the origin and mixing of the water masses in southern Baffin Bay, Davis Strait and Labrador Sea, we apply the mixing model described in Section 2.3. In this section, we first examine the endmembers used in the mixing model (Section 4.1), followed by a discussion of the evolution of West Greenland Shelf Water and West Greenland Irminger Water (WGSW and WGIW) as they enter Baffin Bay (Section 4.2), the origin of Transition Water, Baffin Bay Mode Water and Baffin Bay Bottom Water (BMW, BBBW), cold Arctic Water, and Arctic Water (Sections 4.3 and 4.4) and their evolution to the Labrador Sea (Section 4.5). An overview of the mixing fractions obtained is given in Table A3.

### 4.1 Endmembers in the mixing model

Figure 5A shows the geographical locations of the defined endmembers, each represented with distinct symbols and colours. Their corresponding  $^{129}\text{I}$  and  $^{236}\text{U}$  tracer signatures are displayed in Fig. 5B. The endmembers are defined using a combination

of published data and new tracer measurements. Water mass assignments are based on temperature–salinity characteristics, and for endmembers taken from the literature, the original classifications are retained. Table A2 summarises all endmembers used in this study, including their geographic locations, depth ranges, tracer concentrations, temperature and salinity values, the number of samples included, and the relevant references.

Based on previous studies, the initial mixing scenarios (Fig. 5B) are constructed using the following endmember pairs: AAW<sub>CB</sub> – Pacific Water (Peterson et al., 2012; Lehmann et al., 2022), Nares Strait outflow – Pacific Water (Melling et al., 2008) and WGSW – NAC (North Atlantic Current; Leist et al., 2024).

#### 4.1.1 Endmembers in the subpolar North Atlantic and the Arctic Canada Basin

The NAC endmember (North Atlantic Current; turquoise diamond, Fig. 5) contributes to WGIW and transports mainly subtropical Atlantic water labelled with a low tracer content from global fallout and a small contribution from the European nuclear reprocessing plants (Leist et al., 2024; Castrillejo et al., 2018). Representative of this endmember are samples taken east of Reykjanes Ridge (St. 38, IcSPMW, Castrillejo et al., 2018). The diluted reprocessing plant signal may originate from tracer-labelled water entering the subpolar gyre from the Labrador and Irminger seas and reaching east of the Reykjanes Ridge. The Iceland Scotland Overflow Water (ISOW), formed by deep convection north of Iceland, is represented by data collected before entering the Icelandic Basin on the eastern side of the Reykjanes Ridge (Dale et al., 2024).

The endmember of the Polar Surface Water at the East Greenland Current (PSW<sub>EGC</sub>, dark red diamond, Fig. 5) represents the surface water outflowing the Arctic Ocean at Fram Strait (Wefing et al., 2019), which are then transported south by the East Greenland Current (Fig. 1A). This endmember corresponds to samples collected near the Denmark Strait in 2021 (St. MG17, Dale et al., 2024) and represents surface water entering the Labrador Sea via the West Greenland Current (WGC). As described in Dale et al. (2024) and Leist et al. (2024), the samples most characteristic of PSW<sub>EGC</sub> are located at the shelfbreak of southern Greenland, still containing a significant fraction of PSW (Dale et al., 2024). The PSW<sub>EGC</sub> endmember falls within a dilution line between NAC and the PSW sampled at 100 m depth in the Eurasian Basin (EB) in 2021 by Wefing et al. (2025) (grey circles, Fig. 5, Station Nr. 16, 28, 46 in Wefing et al. (2025)). The PSW<sub>EGC</sub> and PSW<sub>EB</sub> from the Eurasian Basin both represent "younger" water imprinted with post-1980s reprocessing releases (Wefing et al., 2025) with high <sup>129</sup>I and comparably low <sup>236</sup>U due to the shape of the input function of both tracers (Fig. A1).

In contrast, the "old" Arctic Atlantic Water (AAW) in the Arctic Canada Basin (AAW<sub>CB</sub>, grey diamond, Fig. 5), contains high <sup>236</sup>U and comparably low <sup>129</sup>I (Fram Strait Branch Water at St. MK2, MK3 and CB28b, CB29 in Payne et al., 2024). These tracer values correspond to global fallout and reprocessing discharges prior to the 1990s (Fig. A1). Above AAW<sub>CB</sub>, the Pacific Summer Water holds especially low <sup>129</sup>I and <sup>236</sup>U from global fallout alone (dark green diamond in Fig. 5, all stations of JOIS 2020 Payne et al. (2024)).

Freshwater, such as precipitation, river runoff, sea ice melt and glacial meltwater, is referred to as tracer-free and indicated as a diamond with a black outline in Fig. 5B. The Pacific Water, low in salinity, has only elevated <sup>236</sup>U from the global fallout, while the NAC, even though its hydrographic properties are very different, has low tracer concentrations as well. Therefore, it

is not possible to disentangle the different contributions of these water masses using  $^{129}\text{I}$  and  $^{236}\text{U}$  and one should add other tracers such as  $\delta^{18}\text{O}$ . Incorporating such an analysis, however, lies beyond the scope of this study, which focuses specifically on water masses identifiable through radionuclide signatures.

#### 385 4.1.2 Geographical Endmembers in Nares Strait and Lancaster Sound

Based on their geographic location, the 2024 measurements from western Nares Strait (unfilled orange symbols Fig. 5) and southern Lancaster Sound (unfilled red symbols) serve as geographical endmembers for characterising the inflows from the Arctic into Baffin Bay. The surface water at Nares Strait is characterised by low salinity (Fig. A4B) and low tracer concentrations (Fig. 2A and B), both indicative of the inflow of tracer-free water (Münchow et al., 2006; Rabe et al., 2010). In northern Nares  
390 Strait (unfilled orange squares in Fig. 5) at depth below 200 m, high tracer signals were observed, probably as a result of the mixing between the Arctic-Atlantic waters from the Canada Basin (grey diamond in Fig. 5) and PSW originating from the Eurasian Basin, i.e. Amundsen and Makarov basins (grey circle in Fig. 5) (Münchow, Andreas et al., 2007; Jackson et al., 2014; Wefing et al., 2025).

In southern Nares Strait (unfilled orange circles in Fig. 5), downstream of the shallow 220 m sill, tracer concentrations  
395 observed below 150 m are consistent with a mixture of waters advected from northern Nares Strait, mixed with approximately 20% of tracer-free water, and potential contributions of water inflowing Nares Strait from eastern Baffin Bay (Shroyer et al., 2015; Münchow, Andreas et al., 2007; Münchow, Andreas, and Humfrey Melling, 2008). This geographical endmember is illustrated as an orange cross in Fig. 5B), representing the inflowing waters to Baffin Bay.

Similar to Nares Strait, the surface water in southern Lancaster Sound (red symbols in Fig. 5) is composed by Pacific and/or  
400 tracer-free water (Lehmann et al., 2022; McGeehan and Maslowski, 2012), as reflected by its low tracer concentration and salinity. However, Lancaster Sound samples show a stronger influence from  $\text{AAW}_{\text{CB}}$ , as indicated by their position near the  $\text{AAW}_{\text{CB}}$  – Pacific Water mixing line. In 2024, the subsurface waters (10 m - 100 m) of western Lancaster Sound showed the highest  $\text{AAW}_{\text{CB}}$  contribution (55-65%) if mixing with Pacific Water. However, in Lancaster Sound, there is also a slight contribution of waters coming from Nares Strait (Lehmann et al., 2022; Shadwick et al., 2011; Dunlap and Tang, 2006),  
405 which circulate into Lancaster Sound. This is observed in two samples from 140 m and 200 m depth with tracer signals close to the  $\text{NS}_{\text{South}}$  endmember. Samples below 200 m from eastern Lancaster Sound (red unfilled diamonds in Fig. 5B) are strongly influenced by exchanges with Baffin Bay, indicated in temperature above  $0^\circ\text{C}$  (Fig. A2A), probably obtained by double-diffusion with WGIW (Lobb et al., 2003). For the geographical endmember (red cross in Fig. 5B), the station in western Lancaster Sound (red filled triangle) is selected, because it is considered to be more representative of the connectivity to the  
410 Arctic Canada Basin through the CAA. This endmember is calculated from the mean values in the upper 100 m, representative of the CAA outflow and thus excluding potential recirculation entering the Sound from Baffin Bay. However, it is important to note that samples taken in Lancaster Sound were collected two years after the samples in Davis Strait. Since outflow from Lancaster Sound is variable on interannual timescales (Prinsenbergh and Hamilton, 2005), this endmember might not be fully representative of waters found in Baffin Bay. For example, in previous years, Lancaster Sound endmember might have had a  
415 stronger influence of  $\text{AAW}_{\text{CB}}$ , thus carrying a higher  $^{236}\text{U}$  signal.

The presence of AAW<sub>CB</sub> in central CAA has been previously observed using more detailed nutrients and temperature-salinity sampling (Jones et al., 2003; Rudels et al., 2004; Lehmann et al., 2022; Wang et al., 2012; Prinsenbergh and Hamilton, 2005; Peterson et al., 2012; Melling et al., 1984). Despite the shallow passages through the CAA, the AAW<sub>CB</sub> can make its way to Lancaster Sound as a result of the eastward transport by strong winds (Melling et al., 1984), tidal currents and vertical mixing  
420 enhanced by shallow bathymetry (Lehmann et al., 2022; Rudels, 1986; Hughes et al., 2017). The AAW<sub>CB</sub> might further be upwelled to the Archipelago by easterly wind events (Peterson et al., 2012), associated with the Beaufort High or synoptic low-pressure systems originating in the North Pacific. This would result in upwelling of AAW<sub>CB</sub> onto the shallow Chukchi and Beaufort Sea shelves, where AAW<sub>CB</sub> can be transported towards the CAA as part of the Beaufort Sea shelfbreak jet (Pickart et al., 2013; Lin et al., 2019; Yang, 2006; Pickart et al., 2009). Although storms associated with AAW<sub>CB</sub> upwelling are centred  
425 over the Aleutian Islands in the Bering Sea (Pickart et al., 2009), their northward passage into the Beaufort Sea can cause anomalies of cyclonic wind stress over the Canada Basin, which in turn increases volume transports through Lancaster Sound (Zhang et al., 2016; Peterson et al., 2012).

## 4.2 Evolution of West Greenland Shelf Water and West Greenland Irminger Water

430 West Greenland Shelf Water (WGSW) and West Greenland Irminger Water (WGIW) undergo strong seasonal hydrographic variability. They cool and become more saline in winter and freshen in summer, which complicates quantifying their role in water mass formation in Baffin Bay (Curry et al., 2014). In contrast, radionuclide tracers remain unaffected by these processes, making them a powerful tool for tracking WGSW and WGIW in their journey to northern latitudes. In our dataset, the largest hydrographic variations are observed in WGSW: samples from the AR7W Line show low temperatures in spring (overlapping  
435 dark red triangles in Fig. 4A), while autumn samples adjacent to Davis Strait display higher temperatures and a broad salinity range (all dark red symbols in Fig. 4A, with CT above 2°C). Despite these seasonal changes, tracer concentrations (Fig. 4B) remain remarkably stable, enabling a robust quantification of the contribution of WGSW to water mass formation. In the model, mixing between PSW<sub>ECC</sub> – NAC is considered in Fig. 6A for the formation and evolution of WGSW (dark red symbols) and WGIW (light green symbols).

440 Along the AR7W Line (dark red triangles in Fig. 6A) the WGSW retained up to 70% of the PSW<sub>ECC</sub>. As the WGSW flows northward along the Greenland shelf, it becomes progressively entrained by tracer-free water and WGIW (light green symbols in Fig. 6A). By the time WGSW reaches Davis Strait and the Northern Line (diamonds and circles in Fig. 6A), the PSW<sub>ECC</sub> fraction has declined to approximately 40%. This dilution could be compared to the decrease in the thickness of warm Polar Water (equivalent to WGSW) as they flow from eastern Davis Strait to eastern Northern Line, observed by Huang et al. (2024).

445 At central Baffin Bay, water classified as Arctic Water (light brown square in Fig. 6A), preserved a significant fraction (about 30%) of PSW<sub>ECC</sub> compared to the endmember at Denmark Strait. This finding contrasts with Huang et al. (2024) and Lehmann et al. (2022), who did not consider WGSW as a major contributor to the formation of water masses in the region. The substantial presence of WGSW may underscore the role of eddies, the off-branching character of the WGC, and the significant transformation of surface water in Baffin Bay.

450 On the contrary, WGIW is positioned closer to the NAC endmember than WGSW, reflecting a stronger influence from southern-sourced water and thus exhibits lower tracer concentrations. An increase in its tracer content from the Labrador Sea to Baffin Bay confirms its mixing with WGSW, preserving approximately 15%  $PSW_{EGC}$ , consistent with the decrease in the thickness observed by Huang et al. (2024), while contrasting Rysgaard et al. (2020), who did not observe WGIW on the Greenland shelf in Baffin Bay. Furthermore, Huang et al. (2024) observed WGIW in central Baffin Bay, which could not be  
455 identified here, probably due to the limitation of the mixing of two endmembers in the tracer analysis.

### 4.3 Origin of Transition Water, Baffin Bay Mode and Bottom Water

The formation and origin of Transition Water (TrW) remain subjects of ongoing debate. Huang et al. (2024) characterised Transition Water (their TrW1) as a mixture of several water masses, including WGIW, cold Arctic Water and WGSW. In contrast, Rudels (2011) described it as a blend of “Atlantic” water from the south and denser, colder northern water. Complementing  
460 these perspectives, nutrient analyses by Lehmann et al. (2022) and Azetsu-Scott et al. (2010) identified WGIW, Pacific Water, and Arctic-Atlantic Waters as the primary contributors of Transition Water formation.

The broad range of  $^{129}\text{I}$  and  $^{236}\text{U}$  concentrations within Transition Water are consistent with the contribution from multiple endmembers (Huang et al., 2024; Lehmann et al., 2022). The temperature maximum within Transition Water ( $\text{TrW}_{T_{\max}}$ , dark blue symbol in Figs. 4 and 6A) clusters near the Lancaster Sound endmember (red cross in Fig. 6A), whereas the remaining  
465 Transition Water (light blue symbols in Figs. 4 and 6A) exhibits a spread towards lower temperatures and higher  $^{129}\text{I}$ , indicative of additional mixing processes. However, as mentioned above, the Lancaster Sound outflow is known to be highly variable (Lehmann et al., 2022; Peterson et al., 2012; Prinsenber and Hamilton, 2005) and might shift along the Pacific –  $\text{AAW}_{\text{CB}}$  mixing line. Therefore, the contribution of Lancaster Sound outflow to waters in Baffin Bay ( $\text{TrW}_{T_{\max}}$  and  $\text{BBMW}$ ) is not calculated using this geographical endmember but from the mixing line between Pacific –  $\text{AAW}_{\text{CB}}$  endmembers. Although the  
470 Lancaster Sound outflow might not be considered as a fixed endmember, its influence remains apparent in the composition of Transition Water and  $\text{TrW}_{T_{\max}}$ .  $\text{TrW}_{T_{\max}}$  reflects contributions of cold,  $^{236}\text{U}$ -rich  $\text{AAW}_{\text{CB}}$  mixed with Pacific Water from Lancaster Sound, while its elevated temperatures are likely caused by mixing with warm,  $^{129}\text{I}$ - and  $^{236}\text{U}$ -poor WGIW within Baffin Bay. This results in a contribution of the  $\text{AAW}_{\text{CB}}$  of 40–60% if calculated using Pacific water as the lower tracer endmember (i.e. this is a lower bound contribution, as  $\text{TrW}_{T_{\max}}$  also mix with WGIW). This finding aligns with observations  
475 by Lehmann et al. (2022), but emphasises the outflow of Lancaster Sound as more important than contributions by the Nares Strait endmember. This finding differs from Shadwick et al. (2011), who attributed the AAW component to Nares Strait outflow only. The Lancaster Sound outflow might be transported from shallow to intermediate depths by deep convection and cascading driven by intense air–sea fluxes and polynya activity (Wang et al., 2012; Vincent, 2019; Yao and Tang, 2003; Aagaard and Carmack, 1989; Marson et al., 2017), being subsequently redistributed through lateral exchange between slope and basin  
480 waters, as modelled by Münchow et al. (2015). At intermediate depths, particularly along the  $27.5 \text{ kg m}^{-3}$  isopycnal (Lobb et al., 2003; Shan et al., 2024), this dense water may encounter warm WGIW, where diffusive instability and cabbeling promote further mixing and downward propagation (Lobb et al., 2003; Shan et al., 2024; Huang et al., 2024), forming  $\text{TrW}_{T_{\max}}$ .

Ultimately, Transition Water forms through the evolution of  $\text{TrW}_{\text{Tmax}}$  toward colder, fresher waters, which results in less  $^{236}\text{U}$  and higher  $^{129}\text{I}$  due to mixing with WGSW (Figure 6A, dashed line connecting  $\text{TrW}_{\text{Tmax}}$  with WGSW). WGSW may  
485 entrain Transition Water through cascading along the Greenland Shelf (Marson et al., 2017). Additionally, Transition Water might also have contributions from the Nares Strait outflow (Jones et al., 2003), as observed by the increased concentrations  $^{236}\text{U}$  that bring some of the Transition Water to the Nares Strait endmember in Fig. 6A.

Despite the limitations of a two-endmember model to constrain the origin and mixing of water masses, the radionuclide tracers strongly suggest the presence of  $\text{AAW}_{\text{CB}}$  outflowing Lancaster Sound and subsequently entraining Transition Water, a  
490 process that could not be quantified when using nutrient-based tracers alone (Lehmann et al., 2022; Azetsu-Scott et al., 2012). Furthermore, radionuclide tracers show negligible contributions of WGSW to  $\text{TrW}_{\text{Tmax}}$ .

Moving to greater depths, the origin and formation of BBMW still remain unclear (Bourke et al., 1989; Rudels et al., 2004). BBMW (purple symbols in Fig. 6A) has been suggested to be older than other water masses in the region, with tracer ages  
495 estimated to be up to 90 years (Lique et al., 2010), which aligns well with a tracer signal of "old" water according to Fig. A1. The relatively high  $^{236}\text{U}$  and very low  $^{129}\text{I}$  displayed by BBMW indicate the presence of  $\text{AAW}_{\text{CB}}$  and align with observations by Rudels et al. (2004) and Bailey (1956). However, based on the available tracer data, it is not possible to differentiate if the  $\text{AAW}_{\text{CB}}$  originated from Nares Strait, as indicated by Rudels et al. (2004) and Bailey (1956) or from Lancaster Sound.

500 Finally, the deepest waters in Baffin Bay, also known as Baffin Bay Bottom Water (BBBW), remain tracer-free (Fig.4B, dark purple squares). Low tracer concentrations are consistent with observations by Bourke et al. (1989), which show that convection or cascading do not contribute to BBBW formation, and is further consistent with its long ventilation time of up to 455 years based on tritium and  $^3\text{He}$  measurements (Top et al., 1980). Other studies have posited that Atlantic Water from the Canada Basin may contribute to BBBW formation (Rudels, 1986; Rudels et al., 2004), but this interpretation is incompatible  
505 with high tracer concentrations in the Canada Basin (Payne et al., 2024), which would manifest as elevated  $^{129}\text{I}$  and  $^{236}\text{U}$  concentrations in BBBW.

#### 4.4 Origin and formation of Arctic Water and cold Arctic Water

Arctic Water and cold Arctic Water are significant sources of freshwater to the subpolar North Atlantic, and they are strongly influenced by sea ice, glacial meltwater and Pacific water (Huang et al., 2024; Sherwood et al., 2021; Curry et al., 2014; Shan  
510 et al., 2024). However, the composition of these freshwaters as they mix with other water masses in the region remains uncertain. Here,  $^{236}\text{U}$  and  $^{129}\text{I}$  demonstrate that cold Arctic Water is a mixture of Arctic-Atlantic Water outflowing mostly through Nares Strait, Pacific Water, and WGSW, with minor contributions from Lancaster Sound. Arctic Water has a similar origin, but with a stronger influence of tracer-free freshwater. Both Arctic Water and cold Arctic Water are presented in Fig. 6B as light brown and teal symbols, respectively. The new endmember for WGSW is calculated as the mean of the values shown in  
515 Fig. 6A, with the error bars representing the corresponding standard deviation. This endmember includes all samples with concentrations of  $^{129}\text{I}$  below  $240 \times 10^7$  at/kg, selected to best characterise the core of WGSW advecting north beyond Davis Strait.

We consider mixing between Lancaster Sound (to best represent the surface and subsurface inflow) and WGSW (Lehmann et al., 2022); Nares Strait outflow ( $NS_{South}$ ) and Pacific Waters (Jackson et al., 2014). Additionally, potential mixing between Lancaster Sound and NAC and WGSW with NAC (Marson et al., 2017) is indicated as grey solid lines.

520 Cold Arctic Water generally has higher tracer concentrations than Arctic Water and is confined to a cold ( $CT \sim -1.5$  °C) and rather narrow temperature range, while it covers a salinity range between 32.5 and 33.6 (Figs. 4 and A4). Although Huang et al. (2024) observed mixing between cold Arctic Water (their cold Polar Water), meteoric water, and WGIW, our mixing model (Fig. 6B) points to additional water masses involved in its formation. In the following, we examine each contributor in detail, starting with WGSW.

525 In the binary mixing model, cold Arctic Water stretches from the mixing line of Nares Strait South ( $NS_{South}$ ) and tracer-free waters towards the WGSW endmember, suggesting the presence of WGSW in cold Arctic Water as well. The largest contribution of WGSW, approximately 80%, is observed in a sample located at 54 m depth in the middle of the Northern Line (circle in Fig. 6B). WGSW generally follows the main cyclonic circulation (Curry et al., 2011; Azetsu-Scott et al., 2012; Huang et al., 2024), which may cool through air-sea heat exchange in winter (especially in the North Water Polynya) and cascade along the Greenland shelf (Marson et al., 2017), thus reaching the temperature of the cold Arctic Water (Yao and Tang, 2003). In central Baffin Bay (teal square in Fig. 6B), the Nares Strait outflow contributes up to 70% to cold Arctic Water, in agreement with previous observations by Huang et al. (2024); Lehmann et al. (2022) and Melling et al. (2001).

530 Finally, Pacific Water and NAC (Fig. 6B) with low  $^{129}I$  and  $^{236}U$  may contribute to cold Arctic Water as well. While Huang et al. (2024) focused primarily on contributions of WGIW, the radionuclide tracer data is less conclusive, as mixing with either source produces a similar low-tracer signal. At this stage, the binary mixing model reaches its limit, unable to distinguish between these two low-tracer endmembers. Finally, mixing with Arctic Water, as previously noted by Huang et al. (2024), is likely but cannot be precisely quantified here due to similar  $^{129}I$  and  $^{236}U$  signatures of cold Arctic Water and Arctic Water. Overall, the cold Arctic Water cluster reflects a varying blend of water masses described above, showing no such clear trend when looking at hydrographic properties only.

540 Following the assessment of the cold Arctic Water cluster, we turn to Arctic Water to explore its distinct properties and its close association with cold Arctic Water. Although Arctic Water is fresher than cold Arctic Water, both water masses plot closely together in tracer space (light brown and teal symbols in Fig. 6B). Arctic Water appears to be the result of similar sources as cold Arctic Water but with higher contributions of low-tracer water, probably of tracer-free and Pacific origin (Huang et al., 2024; Planat et al., 2025; Sherwood et al., 2021). In Arctic Water, contributions of WGSW are observed in central Baffin Bay (light brown square in Fig. 6B), highlighting the strong stratification in this region. On the western flank of the Northern Line, there is an influx of low tracer water (light brown circles in Fig. 6B), probably due to mixing with 50% of Pacific Water (if mixing between Pacific and  $NS_{South}$  is considered). These mixed waters remain confined within the BIC and are transported southward. Stronger mixing with cold Arctic Water likely occurs near Davis Strait (diamond symbols), illustrating the dynamic conditions in this area (Huang et al., 2024; Tang et al., 2004). Further south in the Northern Labrador Sea Line (star symbols), Arctic Water was likely sampled within the bifurcation of the WGC, showing a WGSW contribution of up to 70% (if mixing with Lancaster Sound outflow is considered). Gou et al. (2022) attributed a southward transport of

550

water confined to the Greenland Coast to an instability of the WGC, which leads to shedding eddies in the northern Labrador Sea. In comparison, at the AR7W Line (triangles), Arctic Water carried by the Labrador Current transports a lower  $^{129}\text{I}$  signal, probably originating from the Nares Strait outflow (up to 70%, again if mixing  $\text{NS}_{\text{South}}$  with Pacific Water is considered).  
555 As the Labrador Current continues southward along the Canada Shelf, two surface samples (red triangles Fig. 6B) originating south west of the AR7W Line suggest further mixing between WGSW, Nares Strait and/or Lancaster Sound outflow and a low tracer component, probably of North Atlantic origin (i.e. NAC). The two surface samples are warmer (CT:  $1.5^\circ\text{C}$ ) and more saline ( $S_A$ : 33.8) than Arctic Water, but colder and fresher than the remaining samples classified as Labrador Sea surface (Fig.4). Possible influences on the main water masses observed in the Labrador Current might include: seasonal variability in  
560 southward velocities at Davis Strait, which are generally highest in summer and lowest in winter (Curry et al., 2014; Myers, 2005; Shan et al., 2024); variability in the outflow of  $\text{AAW}_{\text{CB}}$  via Hudson Strait south of the Northern Labrador Sea Line (Straneo and Saucier, 2008); the presence of eddies and Irminger Rings (Gou et al., 2022).

#### 4.5 Implications on the formation of Labrador Sea Water and North East Atlantic Deep Water

The formation of Labrador Sea Water (LSW) is driven by deep winter convection and associated physical processes (Clarke and  
565 Gascard, 1983), and is modulated by multiple freshwater sources (salinity  $<34.6$ ; Zhang et al. 2021a) that alter its properties (Yashayaev, 2007; Yamamoto-Kawai et al., 2008). The relative contributions of these sources remain uncertain, with most studies focusing on freshwater inputs from boundary currents (Schmidt and Send, 2007; Zhang et al., 2021a). In contrast, artificial radionuclides highlight the potential importance of off-boundary current sources in the formation of both LSW and North East Atlantic Deep Water (NEADW). Insights from  $^{129}\text{I}$  and  $^{236}\text{U}$  tracers suggest that the properties of LSW and  
570 NEADW may be shaped by mixing between BMW, Transition Water (TrW), and the North Atlantic Current (NAC).

In the previous study by Leist et al. (2024) using  $^{129}\text{I}$  and  $^{236}\text{U}$  in the Labrador Sea region, the mixing model reached its limitations when trying to understand the origin of LSW, due to low tracer concentrations and the absence of critical endmembers. Nonetheless, that study showed that  $^{129}\text{I}$ -rich WGSW eddies contribute to LSW as they branch off the WGC and move into the interior of the Labrador Sea (Leist et al., 2024; Hátún et al., 2007; Holliday et al., 2009; Lilly et al., 2003; Chanut  
575 et al., 2008; Pacini and Pickart, 2022). Labrador Sea Water (blue symbols in Fig. 6C) appears to have a significant contribution of WGSW, estimated to be up to 30% (if mixing with the NAC endmember is considered). The influence of WGSW is even stronger, up to 70%, on surface water of the eastern Labrador Sea (light red triangles in Fig. 6C).

Another source of  $^{129}\text{I}$  and  $^{236}\text{U}$  in the LSW could be the Labrador Current, carrying Arctic Water and cold Arctic Water, but contributions to the LSW formation might be relatively small ( $< 10\%$ ), as previously discussed in Myers (2005), Pickart  
580 and Spall (2007), Wang et al. (2018) and Duyck et al. (2025). However, the main LSW cluster observed in Fig. 6C (blue triangles) is located at comparable low  $^{129}\text{I}$  and elevated  $^{236}\text{U}$  concentrations. This suggests that another water mass, richer in  $^{236}\text{U}$  relative to  $^{129}\text{I}$ , is required to account for the observed composition of LSW. This feature, first noted by Castrillejo et al. (2018) and later confirmed by Leist et al. (2024), can now be explained by the influence of the Transition Water outflowing Davis Strait and entraining into LSW.

585 Among the southward-flowing water entering the Labrador Sea, the Transition Water is the only water mass with sufficiently high  $^{236}\text{U}$  concentrations to explain the tracer signature of LSW. To our knowledge, this entrainment of the Transition Water outflowing Baffin Bay into LSW has not been previously considered in the literature. To estimate the contributions of Transition Water a new endmember is derived from the maximum temperature observed in Transition Water ( $\text{TrW}_{\text{Tmax}}$ , dark blue cross in Fig. 6C) with error bars reflecting the variability between samples. As shown by the blue triangles in Fig. 6C, the contribution of  $\text{TrW}_{\text{Tmax}}$  could be as high as 20%. In Davis Strait, long-term moored measurements of temperature and salinity (Fig. A5A, B), and across-strait velocity (2004-2024) at  $60^\circ\text{W}$  and 500 m depth support this view (Fig. A5C). They show a persistent southward flow of Transition Water from Davis Strait into the Labrador Sea from 2004 to 2024, complementing gridded transports for the 2004-2010 period (Curry et al., 2014). These measurements coincide with the  $^{236}\text{U}$  maximum in Davis Strait ( $^{236}\text{U} \sim 17.5 \times 10^6$  at/kg, Fig. 3), demonstrating that the transport towards the Labrador Sea of water fresher than LSW (590 ( $S_A < 34.9$  g/kg) provides both a  $^{236}\text{U}$  and freshwater source for LSW. Once the Transition Water enters the Labrador Sea, it may be entrained with LSW through mixing along-density surfaces (Zou et al., 2020). Furthermore, similar concentrations of  $^{129}\text{I}$  and  $^{236}\text{U}$  between BMW and LSW (Fig. 4) suggest that substantial mixing also occurs between these water masses. As a result, with an average  $S_A < 34.49$  g/kg, BMW can also act as a further freshwater source for LSW. These previously unreported freshwater contributions from Transition Water and BMW to LSW can help shed light on potentially unresolved 600 physical processes in ocean models that contribute to deep convection variability in the Labrador Sea.

Finally, NEADW is a water mass that originates from multiple sources, including ISOW and LSW (Yashayaev, 2007; García-Ibáñez et al., 2015). In the mixing model (yellow triangles in Fig. 6C), NEADW occupies a low-tracer area influenced by several of these water sources, and known to be strongly entrained by ISOW (yellow-green diamond Fig. 6C, from Dale et al. (2024)) while the contribution of DSOW (dark green triangles) is minor (García-Ibáñez et al., 2018). However, the elevated  $^{236}\text{U}$  relative to  $^{129}\text{I}$  is not explained by the endmembers established so far. Our results suggest that Transition Water and/or BMW contribute up to 25% to NEADW when mixing with NAC is considered. During autumn and winter, BMW can enter the deep Labrador Sea as a weak overflow through Davis Strait (Huang et al., 2024; Curry et al., 2014). Once there, it joins the deeper layers and mixes with NEADW. Although the simple two-endmember model used here cannot fully resolve 610 every contribution, particularly under low tracer concentrations and multiple sources, it still provides a valuable first-order approximation. Future work could build on this foundation with a more comprehensive multiparameter analysis.

## 5 Conclusions

This study uses  $^{129}\text{I}$  and  $^{236}\text{U}$  tracers in Baffin Bay, Davis Strait, and the Labrador Sea to better resolve the pathways and transformations of Arctic and Atlantic water. Elevated  $^{236}\text{U}$  in Transition Water reveals that Arctic-Atlantic Water from the 615 Canada Basin contributes significantly (up to 60%) to Transition Water formation, demonstrating that the outflow of Atlantic-derived water, most probably through Lancaster Sound, has been underestimated so far. At the same time, our results show that the West Greenland Shelf Water feeds into Arctic Water (75%) in central Baffin Bay. Cold Arctic Water is influenced by

Nares Strait outflow (up to 70%) at the centre of the bay, while on the eastern side, it contains up to 80% West Greenland Shelf Water. These processes highlight the role of Arctic outflows in the delivery of freshwater to Baffin Bay and the Labrador Sea. South of Davis Strait, our results show that Transition Water provides a notable contribution (up to 20%) to the formation of Labrador Sea Water with potential contributions to North East Atlantic Deep Water. This previously overlooked pathway not only supplies freshwater but also leaves a distinct tracer signature, with direct implications for convection processes in the Labrador Sea and the composition of North East Atlantic Deep Water.

Together, these findings emphasise that Arctic outflows through the Canadian Arctic Archipelago are more important than previously assumed. They shape the transformation of Baffin Bay water masses and exert a significant influence on the ventilation and freshwater budget of the subpolar North Atlantic. This work motivates repeated sampling to understand inter-annual variability, while capturing these processes more accurately in ocean models will be essential for predicting future changes in deep water formation and the stability of the Atlantic Meridional Overturning Circulation.

*Data availability.* The original datasets for this study can be found at the Zenodo database (<https://doi.org/10.5281/zenodo.16914587>). The CTD data of Lancaster Sound and Nares Strait are provided by Amundsen Science Data Collection Amundsen Science Data Collection (2024).

*Author contributions.* LGTL, MC and NC contributed to the conception and design of the study. LGTL performed the data investigation, formal analysis, and wrote the original draft of the manuscript. The investigation and formal analysis were supported by NC and MC. JL contributed substantially to the interpretation of the results. HT, CV and NC performed AMS measurements. NC and MC supervised the study. NC and LGTL acquired funding. KAS, CL and MR supported sample collection during expeditions and provided hydrographic data. All authors contributed to the manuscript revision and approved the submitted version.

*Competing interests.* The authors declare that the research was without a conflict of interest.

*Acknowledgements.* The PI Núria Casacuberta has received funding from the European Research Council (ERC) under the European Union's Horizon 2020 research and innovation programme (TITANICA project, ERC2020-COG 101001451) and from the Swiss National Science Foundation (PR00P2-193091-TRACEATLANTIC). In addition, Lisa Leist received funding from the Swiss Polar Institute (Polar Access Fund, PAF-2022-03). Jed Lenetsky received funding from the U.S. National Science Foundation awards 1902628 and 1902595. KAS is funded through the OFSI fund, Davis Strait Observing System, by Fisheries and Oceans Canada. Maxi Castrillejo acknowledges funding from the Swiss National Science Foundation project CARVICE (2000021E\_214835). The authors acknowledge the chief scientists, the captains and the crew of the R/V Neil Armstrong and the R/V Atlantis. The scientists involved in the sampling are deeply acknowledged. The authors also thank Emmy Hieronimus, who collected the samples at Lancaster Sound aboard of CCGS Amundsen. Kayley Kündig

and Simona Staub are thanked for their contributions to ETH-based laboratories. In addition, the authors acknowledge the entire ASOF community and their contribution through various discussions. Maps were created using cartopy and the GEBCO data product.

## References

- Aagaard, K. and Carmack, E. C.: The role of sea ice and other fresh water in the Arctic circulation, *Journal of Geophysical Research: Oceans*, 650 94, 14 485–14 498, <https://doi.org/10.1029/jc094ic10p14485>, publisher: American Geophysical Union (AGU), 1989.
- Amundsen Science Data Collection: 2024. CTD-Rosette data collected by the CCGS Amundsen in the Canadian Arctic, Processed data. Version [version]. Archived at [www.polardata.ca](http://www.polardata.ca), Canadian Cryospheric Information Network (CCIN), Waterloo, Canada. doi: 10.5884/12713. Accessed on 06.11.2025, 2024.
- Azetsu-Scott, K., Clarke, A., Falkner, K., Hamilton, J., Jones, E. P., Lee, C., Petrie, B., Prinsenber, S., Starr, M., and Yeats, P.: Calcium carbonate saturation states in the waters of the Canadian Arctic Archipelago and the Labrador Sea, *Journal of Geophysical Research: Oceans*, 115, 2009JC005 917, <https://doi.org/10.1029/2009JC005917>, 2010.
- Azetsu-Scott, K., Petrie, B., Yeats, P., and Lee, C.: Composition and fluxes of freshwater through Davis Strait using multiple chemical tracers, *J. Geophys. Res.*, 117, 2012JC008 172, <https://doi.org/10.1029/2012JC008172>, 2012.
- Bailey, W. B.: On the Origin of Deep Baffin Bay Water, *Journal of the Fisheries Research Board of Canada*, 13, 303–308, 660 <https://doi.org/10.1139/f56-020>, 1956.
- Bamber, J. L., Tedstone, A. J., King, M. D., Howat, I. M., Enderlin, E. M., Van Den Broeke, M. R., and Noel, B.: Land Ice Freshwater Budget of the Arctic and North Atlantic Oceans: 1. Data, Methods, and Results, *Journal of Geophysical Research: Oceans*, 123, 1827–1837, <https://doi.org/10.1002/2017JC013605>, 2018.
- Bourke, R. H., Addison, V. G., and Paquette, R. G.: Oceanography of Nares Strait and northern Baffin Bay in 1986 with emphasis on deep and bottom water formation, *J. Geophys. Res.*, 94, 8289–8302, <https://doi.org/10.1029/JC094iC06p08289>, 1989.
- Bower, A. S., Lozier, M. S., Gary, S. F., and Böning, C. W.: Interior pathways of the North Atlantic meridional overturning circulation, *Nature*, 459, 243–247, <https://doi.org/10.1038/nature07979>, 2009.
- Carmack, E. C., Yamamoto-Kawai, M., Haine, T. W. N., Bacon, S., Bluhm, B. A., Lique, C., Melling, H., Polyakov, I. V., Straneo, F., Timmermans, M., and Williams, W. J.: Freshwater and its role in the Arctic Marine System: Sources, disposition, storage, export, and physical and biogeochemical consequences in the Arctic and global oceans, *Journal of Geophysical Research: Biogeosciences*, 121, 675–670 717, <https://doi.org/10.1002/2015jg003140>, publisher: American Geophysical Union (AGU), 2016.
- Casacuberta, N. and Smith, J. N.: Nuclear Reprocessing Tracers Illuminate Flow Features and Connectivity Between the Arctic and Subpolar North Atlantic Oceans, *Annual Review of Marine Science*, 15, 203–221, <https://doi.org/10.1146/annurev-marine-032122-112413>, 2023.
- Casacuberta, N., Masqué, P., Henderson, G., Rutgers van-der Loeff, M., Bauch, D., Vockenhuber, C., Daraoui, A., Walther, C., Synal, H.-A., and Christl, M.: First  $^{236}\text{U}$  data from the Arctic Ocean and use of  $^{236}\text{U}/^{238}\text{U}$  and  $^{129}\text{I}/^{236}\text{U}$  as a new dual tracer, *Earth and Planetary Science Letters*, 440, 127–134, <https://doi.org/10.1016/j.epsl.2016.02.020>, 2016.
- Castrillejo, M., Casacuberta, N., Christl, M., Vockenhuber, C., Synal, H.-A., García-Ibáñez, M. I., Lherminier, P., Sarthou, G., Garcia-Orellana, J., and Masqué, P.: Tracing water masses with  $^{129}\text{I}$  and  $^{236}\text{U}$  in the subpolar North Atlantic along the GEOTRACES GA01 section, *Biogeosciences*, 15, 5545–5564, <https://doi.org/10.5194/bg-15-5545-2018>, 2018.
- 680 Chanut, J., Barnier, B., Large, W., Debreu, L., Penduff, T., Molines, J. M., and Mathiot, P.: Mesoscale Eddies in the Labrador Sea and Their Contribution to Convection and Restratification, *Journal of Physical Oceanography*, 38, 1617–1643, <https://doi.org/10.1175/2008JPO3485.1>, 2008.

- Christl, M., Vockenhuber, C., Kubik, P., Wacker, L., Lachner, J., Alfimov, V., and Synal, H.-A.: The ETH Zurich AMS facilities: Performance parameters and reference materials, *Nuclear Instruments and Methods in Physics Research Section B: Beam Interactions with Materials and Atoms*, 294, 29–38, <https://doi.org/10.1016/j.nimb.2012.03.004>, 2013.
- 685 Christl, M., Casacuberta, N., Vockenhuber, C., Elsässer, C., Bailly du Bois, P., Herrmann, J., and Synal, H.: Reconstruction of the  $^{236}\text{U}$  input function for the Northeast Atlantic Ocean: Implications for  $^{129}\text{I}$ / $^{236}\text{U}$  and  $^{236}\text{U}$ / $^{238}\text{U}$ -based tracer ages, *Journal of Geophysical Research: Oceans*, 120, 7282–7299, <https://doi.org/10.1002/2015JC011116>, 2015.
- Christl, M., Gautschi, P., Maxeiner, S., Müller, A. M., Vockenhuber, C., and Synal, H.-A.:  $^{236}\text{U}$  analyses with the ETH Zurich MILEA prototype system, *Nuclear Instruments and Methods in Physics Research Section B: Beam Interactions with Materials and Atoms*, 534, 61–71, <https://doi.org/10.1016/j.nimb.2022.11.009>, 2023.
- 690 Clarke, R. A. and Gascard, J.-C.: The Formation of Labrador Sea Water. Part I: Large-Scale Processes, *Journal of Physical Oceanography*, 13, 1764 – 1778, [https://doi.org/https://doi.org/10.1175/1520-0485\(1983\)013<1764:TFOLSW>2.0.CO;2](https://doi.org/https://doi.org/10.1175/1520-0485(1983)013<1764:TFOLSW>2.0.CO;2), 1983.
- Cuny, J., Rhines, P. B., Niiler, P. P., and Bacon, S.: Labrador Sea Boundary Currents and the Fate of the Irminger Sea Water, *Journal of Physical Oceanography*, 32, 627–647, [https://doi.org/10.1175/1520-0485\(2002\)032<0627:LSBCAT>2.0.CO;2](https://doi.org/10.1175/1520-0485(2002)032<0627:LSBCAT>2.0.CO;2), 2002.
- 695 Cuny, J., Rhines, P. B., and Ron Kwok: Davis Strait volume, freshwater and heat fluxes, *Deep Sea Research Part I: Oceanographic Research Papers*, 52, 519–542, <https://doi.org/10.1016/j.dsr.2004.10.006>, 2005.
- Curry, B., Lee, C. M., and Petrie, B.: Volume, Freshwater, and Heat Fluxes through Davis Strait, 2004–05\*, *Journal of Physical Oceanography*, 41, 429–436, <https://doi.org/10.1175/2010JPO4536.1>, 2011.
- 700 Curry, B., Lee, C. M., Petrie, B., Moritz, R. E., and Kwok, R.: Multiyear Volume, Liquid Freshwater, and Sea Ice Transports through Davis Strait, 2004–10, *Journal of Physical Oceanography*, 44, 1244 – 1266, <https://doi.org/10.1175/JPO-D-13-0177.1>, 2014.
- Dale, D., Christl, M., Vockenhuber, C., Macrander, A., Ólafsdóttir, S., Middag, R., and Casacuberta, N.: Tracing Ocean Circulation and Mixing From the Arctic to the Subpolar North Atlantic Using the  $^{129}\text{I}$ – $^{236}\text{U}$  Dual Tracer, *JGR Oceans*, 129, e2024JC021 211, <https://doi.org/10.1029/2024JC021211>, 2024.
- 705 Dickson, R. R. and Brown, J.: The production of North Atlantic Deep Water: Sources, rates, and pathways, *Journal of Geophysical Research: Oceans*, 99, 12 319–12 341, <https://doi.org/10.1029/94JC00530>, 1994.
- Dunlap, E. and Tang, C. C.: Modelling the Mean Circulation of Baffin Bay, *Atmosphere-Ocean*, 44, 99–109, <https://doi.org/10.3137/ao.440107>, 2006.
- Duyck, E., Foukal, N. P., and Frajka-Williams, E.: Circulation of Baffin Bay and Hudson Bay waters on the Labrador shelf and into the subpolar North Atlantic, *Ocean Science*, 21, 241–260, <https://doi.org/10.5194/os-21-241-2025>, 2025.
- 710 García-Ibáñez, M. I., Pardo, P. C., Carracedo, L. I., Mercier, H., Lherminier, P., Ríos, A. F., and Pérez, F. F.: Structure, transports and transformations of the water masses in the Atlantic Subpolar Gyre, *Progress in Oceanography*, 135, 18–36, <https://doi.org/10.1016/j.pocean.2015.03.009>, 2015.
- García-Ibáñez, M. I., Pérez, F. F., Lherminier, P., Zunino, P., Mercier, H., and Tréguer, P.: Water mass distributions and transports for the 2014 GEOVIDE cruise in the North Atlantic, *Biogeosciences*, 15, 2075–2090, <https://doi.org/10.5194/bg-15-2075-2018>, 2018.
- 715 Gardner, A. S., Moholdt, G., Wouters, B., Wolken, G. J., Burgess, D. O., Sharp, M. J., Cogley, J. G., Braun, C., and Labine, C.: Sharply increased mass loss from glaciers and ice caps in the Canadian Arctic Archipelago, *Nature*, 473, 357–360, <https://doi.org/10.1038/nature10089>, 2011.
- Gelderloos, R., Katsman, C. A., and Drijfhout, S. S.: Assessing the Roles of Three Eddy Types in Restratifying the Labrador Sea after Deep Convection, *Journal of Physical Oceanography*, 41, 2102–2119, <https://doi.org/10.1175/JPO-D-11-054.1>, 2011.
- 720

- Gou, R., Pennelly, C., and Myers, P. G.: The Changing Behavior of the West Greenland Current System in a Very High-Resolution Model, *Journal of Geophysical Research: Oceans*, 127, <https://doi.org/10.1029/2022JC018404>, 2022.
- Grenier, M., Brown, K., Colombo, M., Belhadj, M., Bacconnais, I., Pham, V., Soon, M., Myers, P., Jeandel, C., and François, R.: Controlling factors and impacts of river-borne neodymium isotope signatures and rare earth element concentrations supplied to the Canadian Arctic Archipelago, *Earth and Planetary Science Letters*, 578, 117–134, <https://doi.org/10.1016/j.epsl.2021.117341>, 2022.
- 725 Haine, T. W., Curry, B., Gerdes, R., Hansen, E., Karcher, M., Lee, C., Rudels, B., Spreen, G., De Steur, L., Stewart, K. D., and Woodgate, R.: Arctic freshwater export: Status, mechanisms, and prospects, *Global and Planetary Change*, 125, 13–35, <https://doi.org/10.1016/j.gloplacha.2014.11.013>, publisher: Elsevier BV, 2015.
- Holland, D. M., Thomas, R. H., De Young, B., Ribergaard, M. H., and Lyberth, B.: Acceleration of Jakobshavn Isbræ triggered by warm subsurface ocean waters, *Nature Geoscience*, 1, 659–664, <https://doi.org/10.1038/ngeo316>, publisher: Springer Science and Business Media LLC, 2008.
- 730 Holliday, N. P., Bacon, S., Allen, J., and McDonagh, E. L.: Circulation and Transport in the Western Boundary Currents at Cape Farewell, Greenland, *Journal of Physical Oceanography*, 39, 1854–1870, <https://doi.org/10.1175/2009JPO4160.1>, 2009.
- Huang, J., Pickart, R. S., Bahr, F., McRaven, L. T., Tremblay, J.-R., Michel, C., Jeansson, E., Kopec, B., Welker, J. M., and Ólafsdóttir, S. R.: Water mass evolution and general circulation of Baffin Bay: Observations from two shipboard surveys in 2021, *Progress in Oceanography*, 735 229, 103–322, <https://doi.org/10.1016/j.pocean.2024.103322>, 2024.
- Hughes, K. G., Klymak, J. M., Hu, X., and Myers, P. G.: Water mass modification and mixing rates in a 1/12° simulation of the Canadian Arctic Archipelago: MIXING IN THE CANADIAN ARCHIPELAGO, *Journal of Geophysical Research: Oceans*, 122, 803–820, <https://doi.org/10.1002/2016JC012235>, 2017.
- 740 Hátún, H., Eriksen, C. C., and Rhines, P. B.: Buoyant Eddies Entering the Labrador Sea Observed with Gliders and Altimetry, *Journal of Physical Oceanography*, 37, 2838–2854, <https://doi.org/10.1175/2007JPO3567.1>, 2007.
- IOC, S. and IAPSO: The international thermodynamic equation of seawater - 2010: Calculation and use of thermodynamic properties., Intergovernmental Oceanographic Commission, Manuals and Guides No. 56, UNESCO (English), 196 pp., [https://www.teos-10.org/pubs/gsw/html/gsw\\_CT\\_from\\_t.html](https://www.teos-10.org/pubs/gsw/html/gsw_CT_from_t.html), 2010.
- 745 Jackson, J. M., Lique, C., Alkire, M., Steele, M., Lee, C. M., Smethie, W. M., and Schlosser, P.: On the waters upstream of Nares Strait, Arctic Ocean, from 1991 to 2012, *Continental Shelf Research*, 73, 83–96, <https://doi.org/10.1016/j.csr.2013.11.025>, 2014.
- Jones, E. P., Swift, J. H., Anderson, L. G., Lipizer, M., Civitarese, G., Falkner, K. K., Kattner, G., and McLaughlin, F.: Tracing Pacific water in the North Atlantic Ocean, *Journal of Geophysical Research: Oceans*, 108, [https://doi.org/https://doi.org/10.1029/2001JC001141](https://doi.org/10.1029/2001JC001141), 2003.
- Komuro, Y. and Hasumi, H.: Intensification of the Atlantic Deep Circulation by the Canadian Archipelago Throughflow, *Journal of Physical Oceanography*, 35, 775–789, <https://doi.org/10.1175/JPO2709.1>, 2005.
- 750 Lavender, K. L., Brechner Owens, W., and Davis, R. E.: The mid-depth circulation of the subpolar North Atlantic Ocean as measured by subsurface floats, *Deep Sea Research Part I: Oceanographic Research Papers*, 52, 767–785, <https://doi.org/10.1016/j.dsr.2004.12.007>, 2005.
- Le Bras, I. A.-A.: Labrador sea water spreading and the Atlantic meridional overturning circulation, *Philosophical Transactions of the Royal Society A: Mathematical, Physical and Engineering Sciences*, 381, 20220189, <https://doi.org/10.1098/rsta.2022.0189>, 2023.
- 755 Lehmann, N., Kienast, M., Granger, J., Bourbonnais, A., Altabet, M. A., and Tremblay, J.: Remote Western Arctic Nutrients Fuel Remineralization in Deep Baffin Bay, *Global Biogeochemical Cycles*, 33, 649–667, <https://doi.org/10.1029/2018GB006134>, 2019.

- Lehmann, N., Kienast, M., Granger, J., and Tremblay, J.: Physical and Biogeochemical Influences on Nutrients Through the Canadian Arctic Archipelago: Insights From Nitrate Isotope Ratios, *Journal of Geophysical Research: Oceans*, 127, e2021JC018179, 760 <https://doi.org/10.1029/2021JC018179>, 2022.
- Leist, L. G. T., Castrillejo, M., Smith, J. N., Christl, M., Vockenhuber, C., Velo, A., Lherminier, P., and Casacuberta, N.: 129I and 236U distribution in the subpolar North Atlantic unravels water mass provenance in AR7W and A25 lines, *Frontiers in Marine Science*, 11, 1470675, <https://doi.org/10.3389/fmars.2024.1470675>, 2024.
- Li, J., Pickart, R. S., Lin, P., Bahr, F., Arrigo, K. R., Juraneck, L., and Yang, X.: The Atlantic Water Boundary Current 765 in the Chukchi Borderland and Southern Canada Basin, *Journal of Geophysical Research: Oceans*, 125, e2020JC016197, <https://doi.org/10.1029/2020JC016197>, 2020.
- Lilly, J. M., Rhines, P. B., Schott, F., Lavender, K., Lazier, J., Send, U., and D'Asaro, E.: Observations of the Labrador Sea eddy field, *Progress in Oceanography*, 59, 75–176, <https://doi.org/10.1016/j.pocean.2003.08.013>, 2003.
- Lin, P., Pickart, R. S., Torres, D. J., and Pacini, A.: Evolution of the Freshwater Coastal Current at the Southern Tip of Greenland, *Journal of* 770 *Physical Oceanography*, 48, 2127–2140, <https://doi.org/10.1175/JPO-D-18-0035.1>, 2018.
- Lin, P., Pickart, R. S., Moore, G., Spall, M. A., and Hu, J.: Characteristics and dynamics of wind-driven upwelling in the Alaskan Beaufort Sea based on six years of mooring data, *Deep Sea Research Part II: Topical Studies in Oceanography*, 162, 79–92, <https://doi.org/10.1016/j.dsr2.2018.01.002>, publisher: Elsevier BV, 2019.
- Lique, C., Treguier, A. M., Blanke, B., and Grima, N.: On the origins of water masses exported along both sides of Greenland: A Lagrangian 775 model analysis, *Journal of Geophysical Research: Oceans*, 115, <https://doi.org/https://doi.org/10.1029/2009JC005316>, 2010.
- Lobb, J., Carmack, E. C., Ingram, R. G., and Weaver, A. J.: Structure and mixing across an Arctic/Atlantic front in northern Baffin Bay, *Geophysical Research Letters*, 30, 2003GL017755, <https://doi.org/10.1029/2003GL017755>, 2003.
- Lozier, M. S.: Overturning in the subpolar North Atlantic: a review, *Philosophical Transactions of the Royal Society A: Mathematical, Physical and Engineering Sciences*, 381, 20220191, <https://doi.org/10.1098/rsta.2022.0191>, 2023.
- 780 Malles, J.-H., Marzeion, B., and Myers, P. G.: Freshwater input from glacier melt outside Greenland alters modeled northern high-latitude ocean circulation, *Earth System Dynamics*, 16, 347–377, <https://doi.org/10.5194/esd-16-347-2025>, 2025.
- Marson, J. M., Myers, P. G., Hu, X., Petrie, B., Azetsu-Scott, K., and Lee, C. M.: Cascading off the W est G reenland S helf: A numerical perspective, *Journal of Geophysical Research: Oceans*, 122, 5316–5328, <https://doi.org/10.1002/2017JC012801>, 2017.
- 785 McGeehan, T. and Maslowski, W.: Evaluation and control mechanisms of volume and freshwater export through the Canadian Arctic Archipelago in a high-resolution pan-Arctic ice-ocean model, *Journal of Geophysical Research: Oceans*, 117, 2011JC007261, <https://doi.org/10.1029/2011JC007261>, 2012.
- Melling, H., Lake, R., Topham, D., and Fissel, D.: Oceanic thermal structure in the western Canadian Arctic, *Continental Shelf Research*, 3, 233–258, [https://doi.org/10.1016/0278-4343\(84\)90010-4](https://doi.org/10.1016/0278-4343(84)90010-4), 1984.
- 790 Melling, H., Gratton, Y., and Ingram, G.: Ocean circulation within the North Water polynya of Baffin Bay, *Atmosphere-Ocean*, 39, 301–325, <https://doi.org/10.1080/07055900.2001.9649683>, 2001.
- Melling, H., Agnew, T. A., Falkner, K. K., Greenberg, D. A., Lee, C. M., Münchow, A., et al.: Fresh-water fluxes via Pacific and Arctic outflows across the Canadian polar shelf, in: *Arctic–Subarctic Ocean Fluxes: Defining the Role of the Northern Seas in Climate*, edited by Dickson, R. R., Meincke, J., and Rhines, P., pp. 193–247, Springer, 2008.

- 795 Myers, P. G.: Impact of freshwater from the Canadian Arctic Archipelago on Labrador Sea Water formation, *Geophys. Res. Lett.*, 32, L06 605, <https://doi.org/10.1029/2004GL022082>, 2005.
- Myers, P. G., Donnelly, C., and Ribergaard, M. H.: Structure and variability of the West Greenland Current in Summer derived from 6 repeat standard sections, *Progress in Oceanography*, 80, 93–112, <https://doi.org/10.1016/j.pocean.2008.12.003>, 2009.
- Münchow, A., Melling, H., and Falkner, K. K.: An Observational Estimate of Volume and Freshwater Flux Leaving the Arctic Ocean through  
800 Nares Strait, *Journal of Physical Oceanography*, 36, 2025–2041, <https://doi.org/10.1175/JPO2962.1>, 2006.
- Münchow, A., Falkner, K. K., and Melling, H.: Baffin Island and West Greenland Current Systems in northern Baffin Bay, *Progress in Oceanography*, 132, 305–317, <https://doi.org/10.1016/j.pocean.2014.04.001>, 2015.
- Münchow, Andreas, Falkner, K.K., and Humfrey Melling: Spatial continuity of measured seawater and tracer fluxes through Nares Strait, a dynamically wide channel bordering the Canadian Archipelago, *Journal of Marine Research*, 65, 759–788, 2007.
- 805 Münchow, Andreas, and Humfrey Melling: Ocean current observations from Nares Strait to the west of Greenland: Interannual to tidal variability and forcing, *Journal of Marine Research*, 66, [https://elischolar.library.yale.edu/journal\\_of\\_marine\\_research/216](https://elischolar.library.yale.edu/journal_of_marine_research/216), 2008.
- Pacini, A. and Pickart, R. S.: Meanders of the West Greenland Current near Cape Farewell, *Deep Sea Research Part I: Oceanographic Research Papers*, 179, 103 664, <https://doi.org/10.1016/j.dsr.2021.103664>, 2022.
- Payne, A.: Anthropogenic Radionuclides as Tracers of Transport, Mixing, Carbon Storage and Freshwater sources in the Canadian Arctic  
810 Ocean, Ph.D. thesis, ETH Zurich, 2026.
- Payne, A., Wefing, A., Christl, M., Vockenhuber, C., Williams, W., Smith, J. N., and Casacuberta, N.: Circulation Timescales and Pathways of Atlantic Water in the Canada Basin: Insights From Transient Tracers <sup>129</sup> I and <sup>236</sup> U, *Journal of Geophysical Research: Oceans*, 129, e2023JC020 813, <https://doi.org/10.1029/2023JC020813>, 2024.
- Pelle, T., Myers, P. G., Hamilton, A., Mazloff, M., Soderlund, K., Beem, L., Blankenship, D. D., Grima, C., Habbal, F., Skidmore, M.,  
815 and Greenbaum, J. S.: Ocean circulation, sea ice, and productivity simulated in Jones Sound, Canadian Arctic Archipelago, between 2003–2016, *EGU sphere*, 2024, 1–34, <https://doi.org/10.5194/egusphere-2024-3751>, 2024.
- Peterson, I., Hamilton, J., Prinsenber, S., and Pettipas, R.: Wind-forcing of volume transport through Lancaster Sound, *Journal of Geophysical Research: Oceans*, 117, <https://doi.org/https://doi.org/10.1029/2012JC008140>, 2012.
- Pickart, R. S. and Spall, M. A.: Impact of Labrador Sea Convection on the North Atlantic Meridional Overturning Circulation, *Journal of*  
820 *Physical Oceanography*, 37, 2207–2227, <https://doi.org/10.1175/JPO3178.1>, 2007.
- Pickart, R. S., Moore, G. W. K., Torres, D. J., Fratantoni, P. S., Goldsmith, R. A., and Yang, J.: Upwelling on the continental slope of the Alaskan Beaufort Sea: Storms, ice, and oceanographic response, *Journal of Geophysical Research: Oceans*, 114, <https://doi.org/10.1029/2008jc005009>, publisher: American Geophysical Union (AGU), 2009.
- Pickart, R. S., Spall, M. A., and Mathis, J. T.: Dynamics of upwelling in the Alaskan Beaufort Sea and associated shelf–basin fluxes, *Deep*  
825 *Sea Research Part I: Oceanographic Research Papers*, 76, 35–51, <https://doi.org/10.1016/j.dsr.2013.01.007>, 2013.
- Planat, N., Tremblay, L. B., Dufour, C. O., and Straub, D.: Seasonal and Decadal Geostrophic Pathways of Pacific and Atlantic Waters in the Arctic Amerasian Basin From Observations, *Journal of Geophysical Research: Oceans*, 130, e2024JC021 560, <https://doi.org/10.1029/2024JC021560>, 2025.
- Polyakov, I. V., Pnyushkov, A. V., Alkire, M. B., Ashik, I. M., Baumann, T. M., Carmack, E. C., Goszczko, I., Guthrie, J., Ivanov, V. V.,  
830 Kanzow, T., Krishfield, R., Kwok, R., Sundfjord, A., Morison, J., Rember, R., and Yulin, A.: Greater role for Atlantic inflows on sea-ice loss in the Eurasian Basin of the Arctic Ocean, *Science*, 356, 285–291, <https://doi.org/10.1126/science.aai8204>, 2017.

- Polyakov, I. V., Pnyushkov, A. V., Charette, M., Cho, K.-H., Jung, J., Kipp, L., Muilwijk, M., Whitmore, L., Yang, E. J., and Yoo, J.: Atlantification advances into the Amerasian Basin of the Arctic Ocean, *Science Advances*, 11, eadq7580, <https://doi.org/10.1126/sciadv.adq7580>, 2025.
- 835 Prinsenbergh, S. and Hamilton, J.: Monitoring the volume, freshwater and heat fluxes passing through Lancaster sound in the Canadian arctic archipelago, *Atmosphere-Ocean*, 43, 1–22, <https://doi.org/10.3137/ao.430101>, 2005.
- Rabe, B., Münchow, A., Johnson, H. L., and Melling, H.: Nares Strait hydrography and salinity field from a 3-year moored array, *Journal of Geophysical Research: Oceans*, 115, 2009JC005966, <https://doi.org/10.1029/2009JC005966>, 2010.
- Rantanen, M., Karpechko, A. Y., Lipponen, A., Nordling, K., Hyvärinen, O., Ruosteenoja, K., Vihma, T., and Laaksonen, A.: The Arctic has  
840 warmed nearly four times faster than the globe since 1979, *Communications Earth & Environment*, 3, 168, <https://doi.org/10.1038/s43247-022-00498-3>, 2022.
- Rhein, M., Steinfeldt, R., Kieke, D., Stendardo, I., and Yashayaev, I.: Ventilation variability of Labrador Sea Water and its impact on oxygen and anthropogenic carbon: a review, *Philosophical Transactions of the Royal Society A: Mathematical, Physical and Engineering Sciences*, 375, 20160321, <https://doi.org/10.1098/rsta.2016.0321>, 2017.
- 845 Rudels, B.: The outflow of polar water through the Arctic Archipelago and the oceanographic conditions in Baffin Bay, *Polar Research*, 4, 161–180, <https://doi.org/10.1111/j.1751-8369.1986.tb00528.x>, 1986.
- Rudels, B.: Volume and freshwater transports through the Canadian Arctic Archipelago–Baffin Bay system, *Journal of Geophysical Research*, 116, C00D10, <https://doi.org/10.1029/2011JC007019>, 2011.
- Rudels, B., Jones, E. P., Anderson, L. G., and Kattner, G.: On the Intermediate Depth Waters of the Arctic Ocean, in: *Geophysical Monograph Series*, edited by Johannessen, O. M., Muench, R. D., and Overland, J. E., pp. 33–46, American Geophysical Union, ISBN 978-1-118-66388-2 978-0-87590-042-1, <https://doi.org/10.1029/GM085p0033>, 1994.
- 850 Rudels, B., Jones, E. P., Schauer, U., and Eriksson, P.: Atlantic sources of the Arctic Ocean surface and halocline waters, *Polar Research*, 23, 181–208, <https://doi.org/10.3402/polar.v23i2.6278>, 2004.
- Rysgaard, S., Boone, W., Carlson, D., Sejr, M. K., Bendtsen, J., Juul-Pedersen, T., Lund, H., Meire, L., and Mortensen, J.: An Updated  
855 View on Water Masses on the pan-West Greenland Continental Shelf and Their Link to Proglacial Fjords, *J. Geophys. Res. Oceans*, 125, <https://doi.org/10.1029/2019JC015564>, 2020.
- Schmidt, S. and Send, U.: Origin and Composition of Seasonal Labrador Sea Freshwater, *Journal of Physical Oceanography*, 37, 1445–1454, <https://doi.org/10.1175/JPO3065.1>, 2007.
- Shadwick, E., Thomas, H., Gratton, Y., Leong, D., Moore, S., Papakyriakou, T., and Prowe, A.: Export of Pacific carbon through the Arctic  
860 Archipelago to the North Atlantic, *Continental Shelf Research*, 31, 806–816, <https://doi.org/10.1016/j.csr.2011.01.014>, 2011.
- Shan, X., Spall, M. A., Pennelly, C., and Myers, P. G.: Seasonal Variability in Baffin Bay, *Journal of Geophysical Research: Oceans*, 129, e2024JC021038, <https://doi.org/https://doi.org/10.1029/2024JC021038>, e2024JC021038 2024JC021038, 2024.
- Sherwood, O. A., Davin, S. H., Lehmann, N., Buchwald, C., Edinger, E. N., Lehmann, M. F., and Kienast, M.: Stable isotope ratios in seawater nitrate reflect the influence of Pacific water along the northwest Atlantic margin, *Biogeosciences*, 18, 4491–4510,  
865 <https://doi.org/10.5194/bg-18-4491-2021>, 2021.
- Shroyer, E. L., Samelson, R. M., Padman, L., and Münchow, A.: Modeled ocean circulation in  $\Delta N$  and its dependence on landfast-ice cover, *Journal of Geophysical Research: Oceans*, 120, 7934–7959, <https://doi.org/10.1002/2015JC011091>, 2015.

- Straneo, F. and Saucier, F.: The outflow from Hudson Strait and its contribution to the Labrador Current, *Deep Sea Research Part I: Oceanographic Research Papers*, 55, 926–946, <https://doi.org/10.1016/j.dsr.2008.03.012>, 2008.
- 870 Sutherland, D. A., Pickart, R. S., Peter Jones, E., Azetsu-Scott, K., Jane Eert, A., and Ólafsson, J.: Freshwater composition of the waters off southeast Greenland and their link to the Arctic Ocean, *Journal of Geophysical Research*, 114, C05 020, <https://doi.org/10.1029/2008JC004808>, 2009.
- Tang, C. C., Ross, C. K., Yao, T., Petrie, B., DeTracey, B. M., and Dunlap, E.: The circulation, water masses and sea-ice of Baffin Bay, *Progress in Oceanography*, 63, 183–228, <https://doi.org/10.1016/j.pocean.2004.09.005>, 2004.
- 875 Tanhua, T.: Spreading of overflow water from the Greenland to the Labrador Sea, *Geophys. Res. Lett.*, 32, L10 605, <https://doi.org/10.1029/2005GL022700>, 2005.
- The IMBIE Team: Mass balance of the Greenland Ice Sheet from 1992 to 2018, *Nature*, 579, 233–239, <https://doi.org/10.1038/s41586-019-1855-2>, 2020.
- 880 Top, Z., Clarke, W. B., Eismont, W. C., and Jones, E. P.: Radiogenic helium in Baffin Bay bottom water, *Journal of Marine Research*, 38, 435–452, [https://elischolar.library.yale.edu/journal\\_of\\_marine\\_research/1514](https://elischolar.library.yale.edu/journal_of_marine_research/1514), 1980.
- Vandecrux, B., Fausto, R. S., Box, J. E., Covi, F., Hock, R., Rennermalm, A. K., Heilig, A., Abermann, J., Van As, D., Bjerre, E., Fettweis, X., Smeets, P. C. J. P., Kuipers Munneke, P., Van Den Broeke, M. R., Brils, M., Langen, P. L., Mottram, R., and Ahlstrom, A. P.: Recent warming trends of the Greenland ice sheet documented by historical firn and ice temperature observations and machine learning, *The Cryosphere*, 18, 609–631, <https://doi.org/10.5194/tc-18-609-2024>, 2024.
- 885 Vincent, R. F.: A Study of the North Water Polynya Ice Arch using Four Decades of Satellite Data, *Scientific Reports*, 9, 20 278, <https://doi.org/10.1038/s41598-019-56780-6>, 2019.
- Vockenhuber, C., Casacuberta, N., Christl, M., and Synal, H.-A.: Accelerator Mass Spectrometry of  $^{129}\text{I}$  towards its lower limits, *Nuclear Instruments and Methods in Physics Research Section B: Beam Interactions with Materials and Atoms*, 361, 445–449, <https://doi.org/10.1016/j.nimb.2015.01.061>, 2015.
- 890 Wang, H., Legg, S., and Hallberg, R.: The Effect of Arctic Freshwater Pathways on North Atlantic Convection and the Atlantic Meridional Overturning Circulation, *J. Climate*, 31, 5165–5188, <https://doi.org/10.1175/JCLI-D-17-0629.1>, 2018.
- Wang, Q., Myers, P. G., Hu, X., and Bush, A. B.: Flow Constraints on Pathways through the Canadian Arctic Archipelago, *Atmosphere-Ocean*, 50, 373–385, <https://doi.org/10.1080/07055900.2012.704348>, 2012.
- 895 Wang, Q., Shu, Q., Wang, S., Beszczynska-Moeller, A., Danilov, S., Steur, L., Haine, T. W. N., Karcher, M., Lee, C. M., Myers, P. G., Polyakov, I. V., Provost, C., Skagseth, t., Spreen, G., and Woodgate, R.: A Review of Arctic–Subarctic Ocean Linkages: Past Changes, Mechanisms, and Future Projections, *Ocean-Land-Atmos Res*, 2, 0013, <https://doi.org/10.34133/olar.0013>, 2023.
- Wang, Q., Shu, Q., and Wang, F.: Recent emergence of Arctic atlantification dominated by climate warming, *Science Advances*, 10, eadq5235, <https://doi.org/10.1126/sciadv.adq5235>, 2024.
- 900 Wefing, A., Christl, M., Vockenhuber, C., Rutgers van der Loeff, M., and Casacuberta, N.: Tracing Atlantic Waters Using  $^{129}\text{I}$  in the Fram Strait in 2016, *Journal of Geophysical Research: Oceans*, 124, 882–896, <https://doi.org/10.1029/2018JC014399>, 2019.
- Wefing, A.-M., Casacuberta, N., Christl, M., Gruber, N., and Smith, J. N.: Circulation timescales of Atlantic Water in the Arctic Ocean determined from anthropogenic radionuclides, *Ocean Science*, 17, 111–129, <https://doi.org/10.5194/os-17-111-2021>, 2021.
- Wefing, A.-M., Payne, A., Scheiwiller, M., Vockenhuber, C., Christl, M., Tanhua, T., and Casacuberta, N.: Changes in Atlantic 905 Water circulation in the central Arctic Ocean between 2011 and 2021 inferred from tracer observations, *EGUsphere*, pp. 1–44, <https://doi.org/10.5194/egusphere-2025-1322>, 2025.

- Weijer, W., Haine, T. W. N., Siddiqui, A. H., Cheng, W., Veneziani, M., and Kurtakoti, P.: INTERACTIONS BETWEEN THE ARCTIC MEDITERRANEAN AND THE ATLANTIC MERIDIONAL OVERTURNING CIRCULATION: A REVIEW, *Oceanography*, 35(3/4), 118–127, <https://www.jstor.org/stable/27182704>, 2022.
- 910 Yamamoto-Kawai, M., McLaughlin, F. A., Carmack, E. C., Nishino, S., and Shimada, K.: Freshwater budget of the Canada Basin, Arctic Ocean, from salinity,  $\delta^{18}\text{O}$ , and nutrients, *Journal of Geophysical Research: Oceans*, 113, 2006JC003858, <https://doi.org/10.1029/2006JC003858>, 2008.
- Yang, J.: The Seasonal Variability of the Arctic Ocean Ekman Transport and Its Role in the Mixed Layer Heat and Salt Fluxes, *Journal of Climate*, 19, 5366–5387, <https://doi.org/10.1175/jcli3892.1>, publisher: American Meteorological Society, 2006.
- 915 Yao, T. and Tang, C. L.: The formation and maintenance of the North Water Polynya, *Atmosphere-Ocean*, 41, 187–201, <https://doi.org/10.3137/ao.410301>, 2003.
- Yashayaev, I.: Changing freshwater content: Insights from the subpolar North Atlantic and new oceanographic challenges, *Progress in Oceanography*, 73, 203–209, <https://doi.org/10.1016/j.pocean.2007.04.014>, 2007.
- Yashayaev, I.: Intensification and shutdown of deep convection in the Labrador Sea were caused by changes in atmospheric and freshwater  
920 dynamics, *Communications Earth & Environment*, 5, 156, <https://doi.org/10.1038/s43247-024-01296-9>, 2024.
- Zhang, J., Weijer, W., Steele, M., Cheng, W., Verma, T., and Veneziani, M.: Labrador Sea freshening linked to Beaufort Gyre freshwater release, *Nature Communications*, 12, 1229, <https://doi.org/10.1038/s41467-021-21470-3>, 2021a.
- Zhang, Y., Chen, C., Beardsley, R. C., Gao, G., Lai, Z., Curry, B., Lee, C. M., Lin, H., Qi, J., and Xu, Q.: Studies of the Canadian Arctic Archipelago water transport and its relationship to basin-local forcings: Results from AO-FVCOM, *Journal of Geophysical Research: Oceans*, 121, 4392–4415, <https://doi.org/10.1002/2016JC011634>, 2016.  
925
- Zhang, Y., Chen, C.-S., Shen, X.-Y., Xu, D.-Y., Shao, W.-Z., Beardsley, R. C., Chang, L., and Feng, G.-P.: Role of sea level pressure in variations of the Canadian Arctic Archipelago throughflow, *Advances in Climate Change Research*, 12, 539–552, <https://doi.org/10.1016/j.accre.2021.07.009>, 2021b.
- Zou, S., Lozier, M. S., Li, F., Abernathy, R., and Jackson, L.: Density-compensated overturning in the Labrador Sea, *Nature Geoscience*,  
930 13, 121–126, <https://doi.org/10.1038/s41561-019-0517-1>, 2020.
- Zou, S., Bower, A. S., Lozier, M. S., and Furey, H. H.: Deep ocean circulation in the subpolar North Atlantic observed by acoustically-tracked floats, *Progress in Oceanography*, 211, 102975, <https://doi.org/10.1016/j.pocean.2023.102975>, 2023.
- Zou, S., Petit, T., Li, F., and Lozier, M. S.: Observation-Based Estimates of Water Mass Transformation and Formation in the Labrador Sea, *Journal of Physical Oceanography*, 54, 1411–1429, <https://doi.org/10.1175/JPO-D-23-0235.1>, 2024.
- 935 Zweng, M. M. and Münchow, A.: Warming and freshening of Baffin Bay, 1916–2003, *Journal of Geophysical Research: Oceans*, 111, 2005JC003093, <https://doi.org/10.1029/2005JC003093>, 2006.

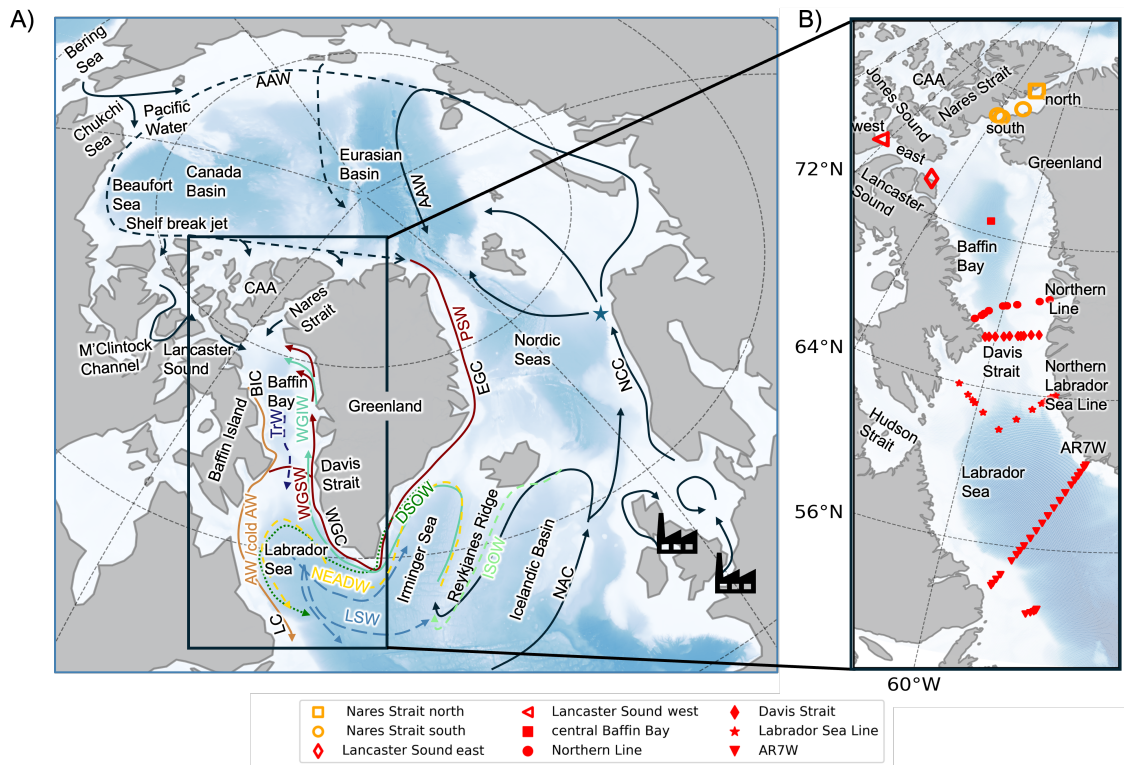


**Figure 1.** **A)** Map of the study area showing the main surface water mass circulation as solid lines, intermediate-depth circulation as dashed lines, and deep circulation as dotted lines, adapted from Curry et al. (2014), García-Ibáñez et al. (2015) and Dale et al. (2024). Ocean current names are shown in black font, while specific water mass names are represented in other colours. Black icons indicate the locations of nuclear fuel reprocessing plants at Sellafield (UK) and La Hague (France), and the blue star marks the location where the tracers input function is defined (Fig. A1). **B)** Close-up view highlighting regional geographic features and the oceanographic transects sampled in this study. Filled red symbols indicate sampling locations surrounding Davis Strait and along AR7W in 2022: central Baffin Bay (square), Northern Line (dots), Davis Strait (diamonds), Northern Labrador Sea Line (stars), and AR7W (triangles). Unfilled red symbols represent samples from Lancaster Sound (west: triangle, east: diamond), while unfilled orange symbols represent samples from Nares Strait (north: square, south: circles). All abbreviations are defined in Appendix Table A1.

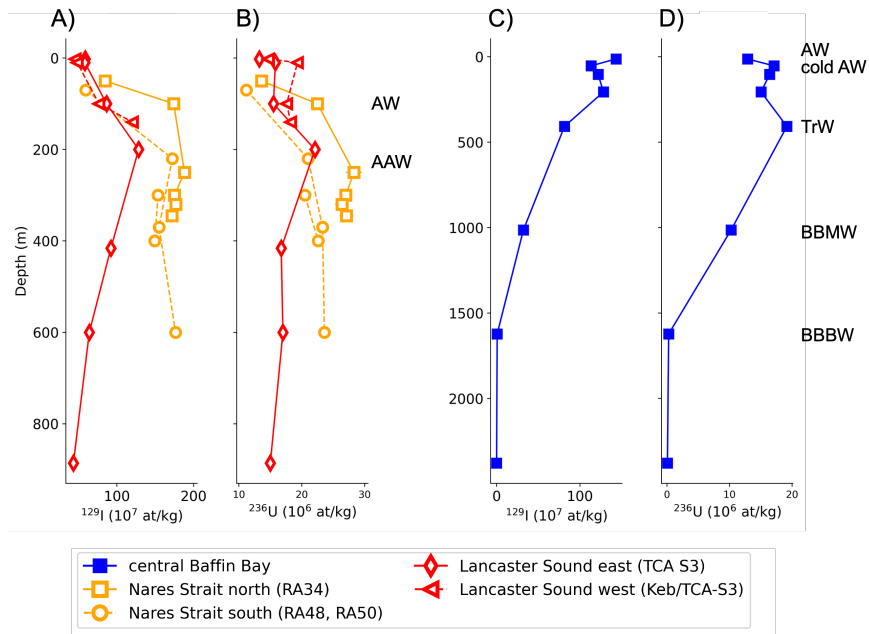


**Figure 2.** Concentration depth profiles in Nares Strait (orange) and Lancaster Sound (red) for  $^{129}\text{I}$  (A) and  $^{236}\text{U}$  (B).  $^{129}\text{I}$  (C) and  $^{236}\text{U}$  (D) depth profiles in central Baffin Bay.

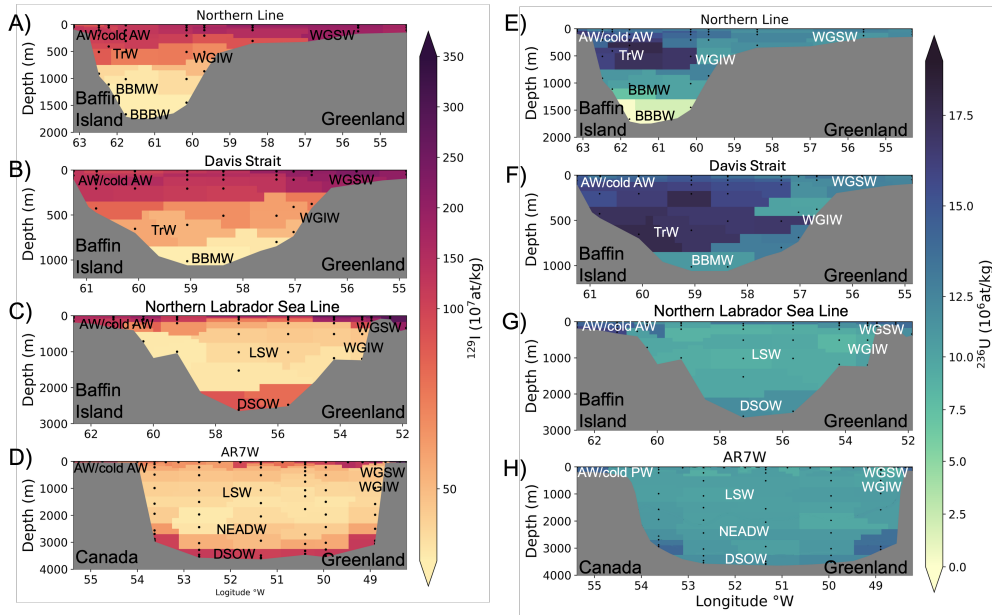


**Figure 3.** Zonal distribution of  $^{129}\text{I}$  (A – D) and  $^{236}\text{U}$  concentrations (E – H) along Northern Line (A, E), Davis Strait (B, F), Northern Labrador Sea Line (C, G) and AR7W (D, H), respectively, in 2022. The water masses are based on Curry et al. (2014), Yashayaev (2007), and Huang et al. (2024).

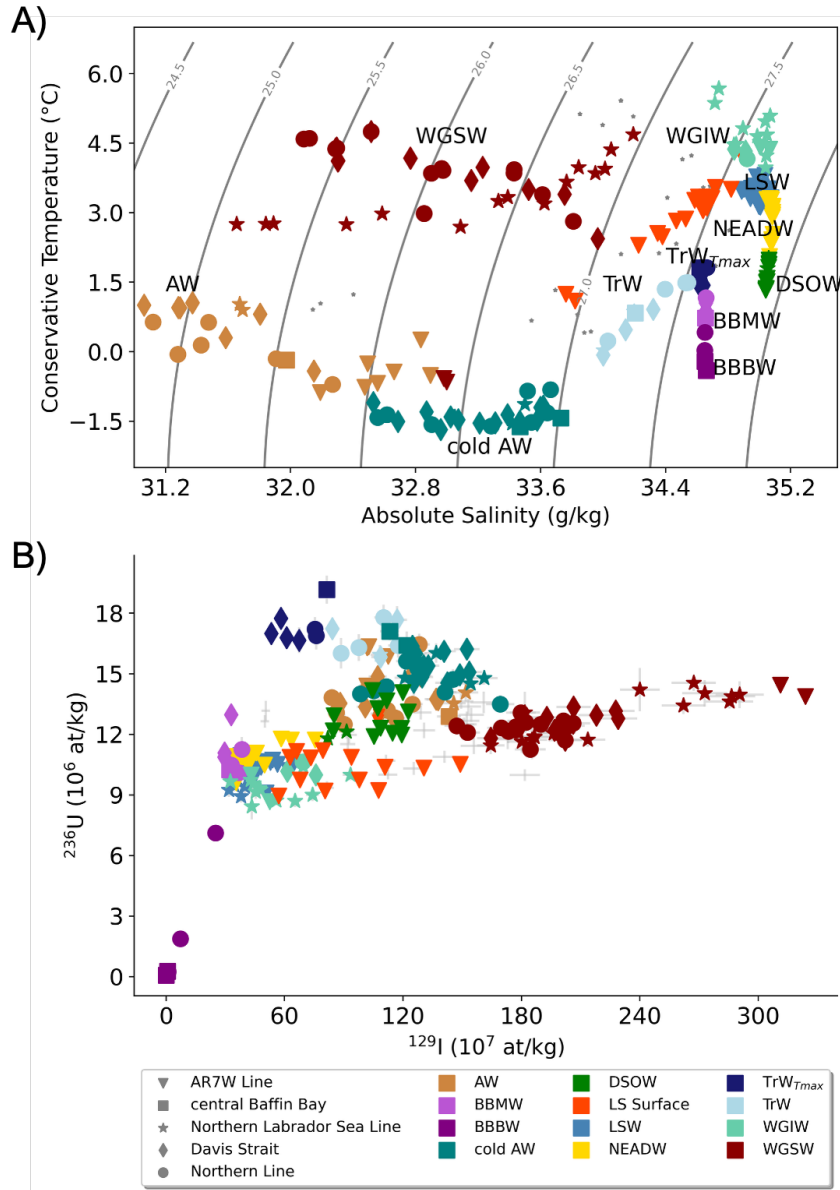


**Figure 4.** Overview of hydrographic and tracer data. **A)** Temperature-salinity (T-S) diagram, showing the distribution of water masses as listed in Table A1. **B)**  $^{129}\text{I}$  vs.  $^{236}\text{U}$  plot for all samples. The same colour coding is used for water masses in A and B, while grey stars represent samples that could not be assigned to a certain water mass. The grey crosses indicate the sample uncertainty. The symbols marking the sampling locations match those in Fig. 1B).

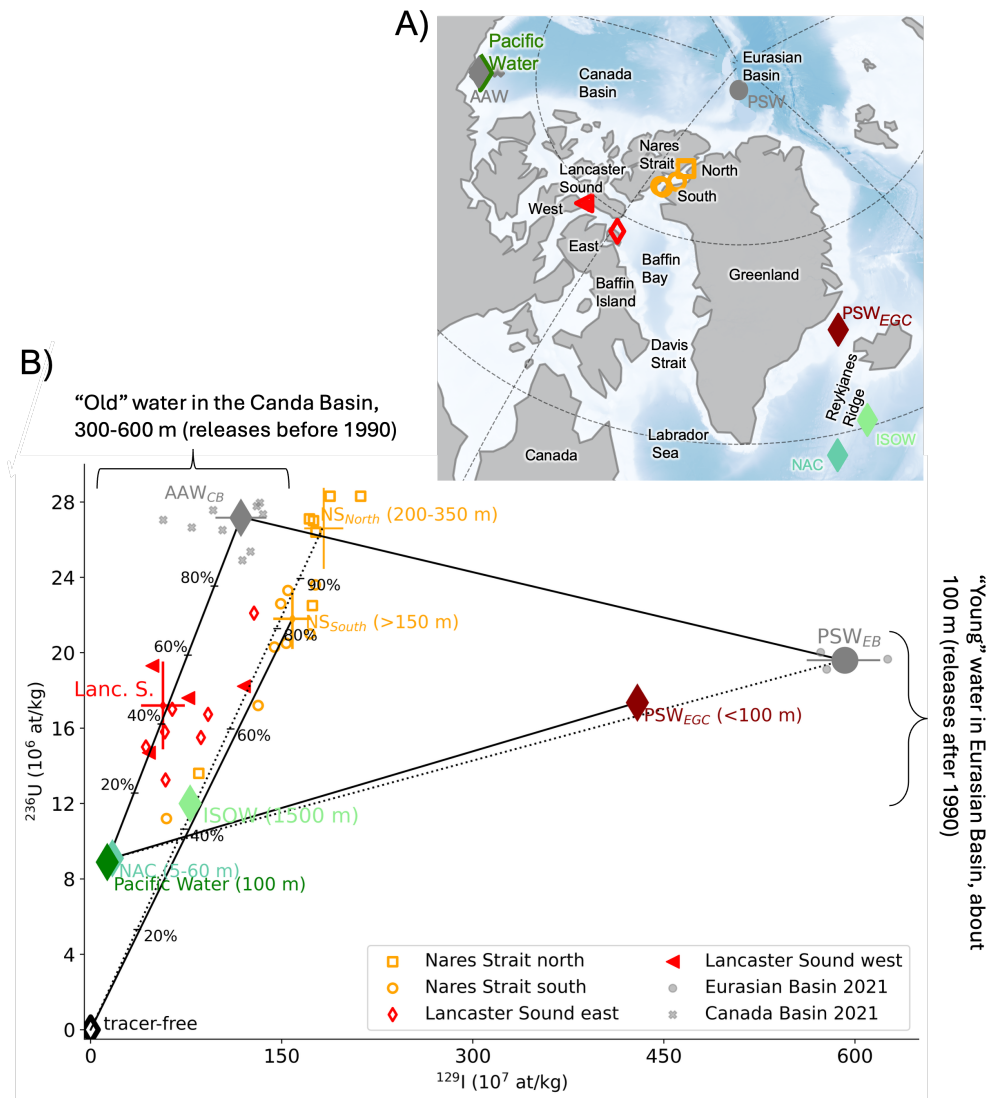


**Figure 5.** Symbols and colours in panels **A)** and **B)** consistently denote water mass endmembers (colored diamonds and circle), previously published Arctic Ocean data (grey diamond and circle), and new data from Lancaster Sound (red symbols) and Nares Strait (orange symbols). **A)** Geographic distribution of endmembers and sampling locations in the Arctic Ocean, Nares Strait, and Lancaster Sound. **B)**  $^{129}\text{I}$ – $^{236}\text{U}$  tracer space showing endmembers and individual samples at Nares Strait and Lancaster Sound. Red crosses indicate the mean and maximum spread of measurements from the upper 100 m in western Lancaster Sound, while the orange cross represents the mean and maximum spread of samples from southern Nares Strait collected below 150 m. Numbers adjacent to the endmembers denote the depth ranges of the samples used in their calculation. AAW<sub>CB</sub>: Arctic Atlantic Water in Canada Basin (Payne et al., 2024). NAC: North Atlantic current (Castrillejo et al., 2018). PSW<sub>EGC</sub>: Polar Surface Water at the East Greenland Current (Dale et al., 2024). Pacific Water (Payne et al., 2024). PSW<sub>EB</sub>: Polar Surface Water in the Eurasian Basin (Wefing et al., 2025). Tracer-free: very old water without anthropogenic signature, glacier and sea ice melt, river runoff, and precipitation.

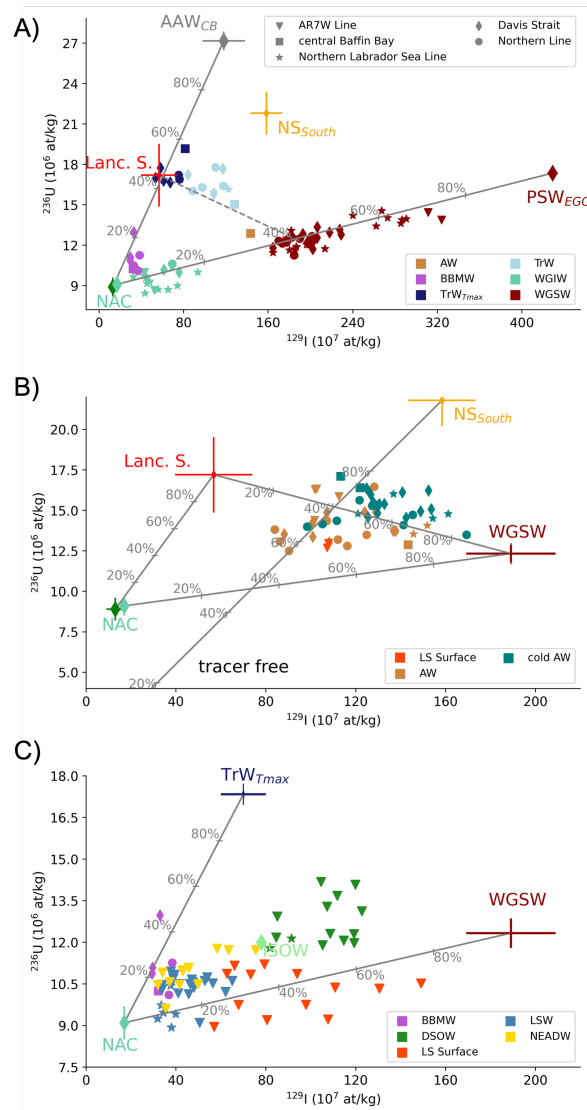


**Figure 6.** Binary mixing model of  $^{129}\text{I}$  vs.  $^{236}\text{U}$  used to infer water mass origins and mixing. Symbol shapes indicate sampling locations: central Baffin Bay (squares), Northern Line (dots), Davis Strait (diamonds), Northern Labrador Sea Line (stars), and AR7W (triangles). Colored diamonds mark endmembers, with crosses showing endmembers defined in this study, including their maximum spread. The line connecting the endmembers represent mixing lines, while number along the mixing lines denotes the mixing fraction. The water masses presented in the panels are selected based on their tracer properties. **A)** Maximum tracer concentrations in the study region are represented by West Greenland Shelf Water (WGSW), West Greenland Irminger Water (WGIW), and Baffin Bay Mode Water (BBMW). Additionally, Transition Water (TrW) is also represented with special emphasis on its temperature maximum ( $\text{TrW}_{T_{\max}}$  dark blue symbols). **B)** Mixing between Arctic Water (AW) and cold Arctic Water (cold AW) in Baffin Bay. **C)** Mixing in the Labrador Sea, including: Labrador Sea Water (LSW), Labrador Sea Surface Water, and North East Atlantic Deep Water (NEADW). References, sample counts, and sampling years for endmembers are listed in Appendix Table A2. Abbreviations are explained in Appendix Table A1.



**Table A1.** Appendix A: Abbreviations of water masses and currents cited in the manuscript. Water mass definitions are based on classifications from Curry et al. (2014), Huang et al. (2024), García-Ibáñez et al. (2015), Yashayaev (2007) and Bourke et al. (1989). In this work, hydrographic properties are reported as follows: Absolute salinity ( $S_A$ , g/kg) and conservative temperature (CT, °C) are given for all data newly analysed in this study, following TEOS-10 recommendations. For water masses described in the literature whose properties were not re-evaluated here, values are reported as practical salinity and potential temperature ( $T_{pot}$ , °C), following the original sources. This approach ensures consistency with both current standards (TEOS-10) and historical literature for all water mass and current definitions.

Acronym	Water mass / current	Salinity	Temperature	Reference
AAW <sub>CB</sub>	Arctic Atlantic Water Canada Basin	$>34.7$	$T_{pot}>0$	Payne et al. (2024)
AAW <sub>CAA</sub>	Arctic Atlantic Water	$S_A > 33$	CT < -1	this study
AW	Arctic Water	$S_A > 32.9$	CT: -0.8 – 1.1	this study
AW <sub>CAA</sub>	Arctic Water CAA	$S_A < 33$	CT < 0	this study
BBBW	Baffin Bay Bottom Water	$S_A: 34.6$	CT < 0.4	this study
BBMW	Baffin Bay Mode Water	$S_A: 34.6$	CT: 0.7 – 1.2	this study
cold AW	cold Arctic Water	$S_A: 32.5 – 33.8$	CT < -0.8	this study
DSOW	Denmark Strait Overflow Water	$S_A < 35 \pm 0.1$	CT < 1.3	this study
ISOW	Iceland–Scotland Overflow Water	34.9–35 PSU	$T_{pot}: 2.0 – 3.5$	Dale et al. (2024)
LSW	Labrador Sea Water	$S_A > 35$	CT: 3.1 – 3.8	this study
NEADW	North East Atlantic Deep Water	$35.07 \pm 0.2$	CT: 2.0 – 3.3	this study
Pacific Water	Pacific Water	<32.5 PSU	$T_{pot} - 0.4 \pm 0.1$	Payne et al. (2024)
PSW <sub>EB</sub>	Polar Surface Water Eurasian Basin	density: $\sigma_\theta < 27.70$		Wefing et al. (2025)
PSW <sub>EGC</sub>	Polar Surface Water at Denmark Strait	<34.3 PSU	$T_{pot} < 0$	Dale et al. (2024)
SAIW	Subarctic Intermediate Water	34.9 PSU	$T_{pot}: 4 – 7$	Castrillejo et al. (2018)
TrW	Transition Water	$S_A: 34.0 – 34.6$	CT: 0 – 1.8	this study
TrW <sub>Tmax</sub>	Temperature maximum in TrW	$S_A: 34.64 \pm 0.03$	CT: 1.4 – 1.8	this study
WGIW	West Greenland Irminger Water	$S_A > 34.7$	CT > 3.5	this study
WGSW	West Greenland Shelf Water	$S_A < 34.2$	CT < 5	this study
BIC	Baffin Island Current			
CAA	Canadian Arctic Archipelago			
EB	Eurasian Basin			
EGC	East Greenland Current			
Lanc. S.	Lancaster Sound			
LC	Labrador Current			
LS	Labrador Sea			
NAC	North Atlantic Current			
NCC	Norwegian Coastal Current			
NS <sub>South</sub>	southern Nares Strait			
WGC	West Greenland Current			

**Table A2.** Endmember data with geographic location and depth, concentrations of  $^{129}\text{I}$  and  $^{236}\text{U}$  and hydrographic properties.

Endmember	Latitude °N	Longitude °E	Depth (m)	$^{129}\text{I}$ ( $\times 10^7$ at/kg)	$^{236}\text{U}$ ( $\times 10^6$ at/kg)	$S_A$	CT	# Samples	Ref
AAW <sub>CB</sub>	70.6 – 77.7	-140.0 – -146.8	300 – 600	$118 \pm 20$	$27.2 \pm 0.7$	$34.96 \pm 0.06$	$0.5 \pm 0.2$	13	a
ISOW	55.3	-26.4	1500	$78 \pm 2$	$12.0 \pm 0.1$	$35.14 \pm 0.01$	$2.7 \pm 0.1$	3	b
Lanc. S.	74.1	-91.1	$\leq 100$	$57 \pm 17$	$17.2 \pm 2.3$	$31.4 \pm 1.33$	$-0.4 \pm 0.7$	d	
NAC	58.5	-31.2	5 – 60	$16.9 \pm 0.4$	$9.1 \pm 0.6$	$35.23 \pm 0.01$	$8.8 \pm 0.7$	3	c
NS <sub>South</sub>	78.3	-73.3 – -74.7	> 150	$158 \pm 15$	$21.8 \pm 1.6$	$33.9 \pm 0.4$	$-0.1 \pm 0.4$	6	d
Pacific	70.6 – 77.7	-140.0 – -146.8	100	$8.5 \pm 2.4$	$4.6 \pm 1.1$	$32.13 \pm 0.25$	$-0.7 \pm 0.4$	8	a
PSW <sub>EGC</sub>	67.5	-25.8	< 100	$429 \pm 5$	$17.3 \pm 0.3$	$33 \pm 1$	$1.2 \pm 3.8$	2	b
WGSW	63.7 – 69.2	-53.0 – -58.4	400 – 650	$189 \pm 20$	$12.3 \pm 0.5$	$33.2 \pm 0.6$	$3.8 \pm 0.6$	30	d
TrW	66.7 – 72.7	-57.3 – -65.9	5 – 300	$70 \pm 10$	$17 \pm 0.1$	$34.6 \pm 0.2$	$1.6 \pm 0.2$	7	d

a: Payne et al. (2024), b: Dale et al. (2024), c: Castrillejo et al. (2018), d: this study.

**Table A3.** Water mass fractions and associated endmembers. Fractions have been calculated using equation 1 (see methods section) and results represent the fractions  $f$  of the water mass described in the first column. Vector  $\vec{b}$  is the distance between the sample and the endmember indicated in the second column (or cluster of samples) and in Fig. 6, and vector  $\vec{a}$  is defined by the two endmembers described in the third column of the table.

<b>Water mass and location</b>	<b>Fraction <math>f</math></b>	<b>Mixing line <math>\vec{b}</math></b>
NS <sub>South</sub>	up to 25% NS <sub>North</sub>	NS <sub>North</sub> – Pacific
Lancaster Sound	55-65% AAW <sub>CB</sub>	AAW <sub>CB</sub> – Pacific
WGSW <sub>AR7W</sub>	up to 70% PSW <sub>EGC</sub>	PSW <sub>EGC</sub> – NAC
WGSW <sub>Davis Strait</sub>	40% PSW <sub>EGC</sub>	PSW <sub>EGC</sub> – NAC
WGIW <sub>Davis Strait</sub>	15% PSW <sub>EGC</sub>	PSW <sub>EGC</sub> – NAC
AW <sub>central Baffin Bay</sub>	75% WGSW	WGSW – NAC
AW <sub>BIC</sub>	55% WGSW	Lanc. S. – WGSW
AW <sub>Labrador Current</sub>	70% NS <sub>South</sub>	NS <sub>South</sub> – Pacific
cold AW <sub>central Baffin Bay</sub>	70% NS <sub>South</sub>	NS <sub>South</sub> – Pacific
cold AW <sub>Northern Line</sub>	80% WGSW	WGSW – NAC
TrW <sub>Tmax</sub>	60-65% AAW <sub>CB</sub>	AAW <sub>CB</sub> – Pacific
LSW	up to 30% WGSW	WGSW – NAC
LSW	up to 20% TrW <sub>Tmax</sub>	TrW <sub>Tmax</sub> – WGIW
LS Surface	up to 70% WGSW	WGSW – NAC
NEADW	up to 25% TrW <sub>Tmax</sub>	TrW <sub>Tmax</sub> – WGIW

## A2 Appendix B, Additional Figures

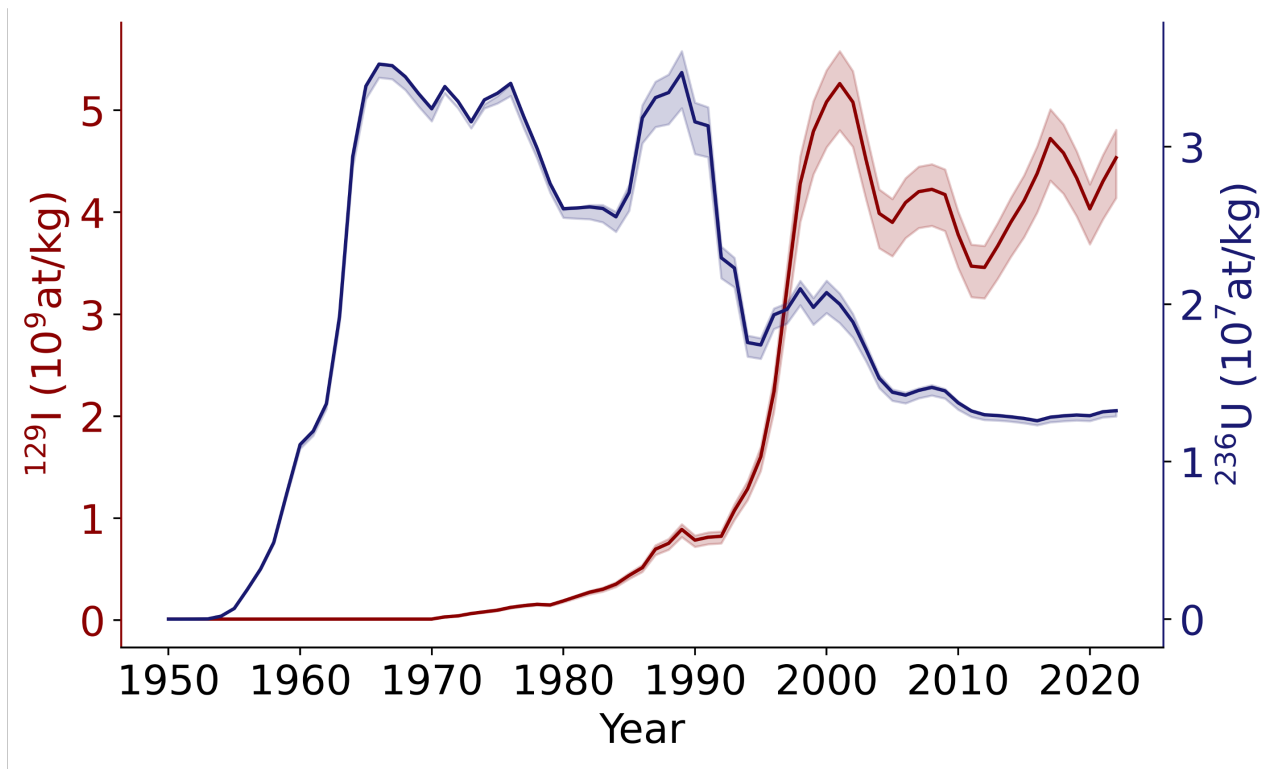


**Figure A1.** Input function of  $^{129}\text{I}$  (red) and  $^{236}\text{U}$  (blue) defined at  $70^\circ\text{N}$  in northern Norway showing the combined input from nuclear fuel reprocessing plants in Sellafield (UK) and La Hague (F), and the global fallout from atmospheric nuclear weapon tests (Wefing et al., 2021; Payne et al., 2024).

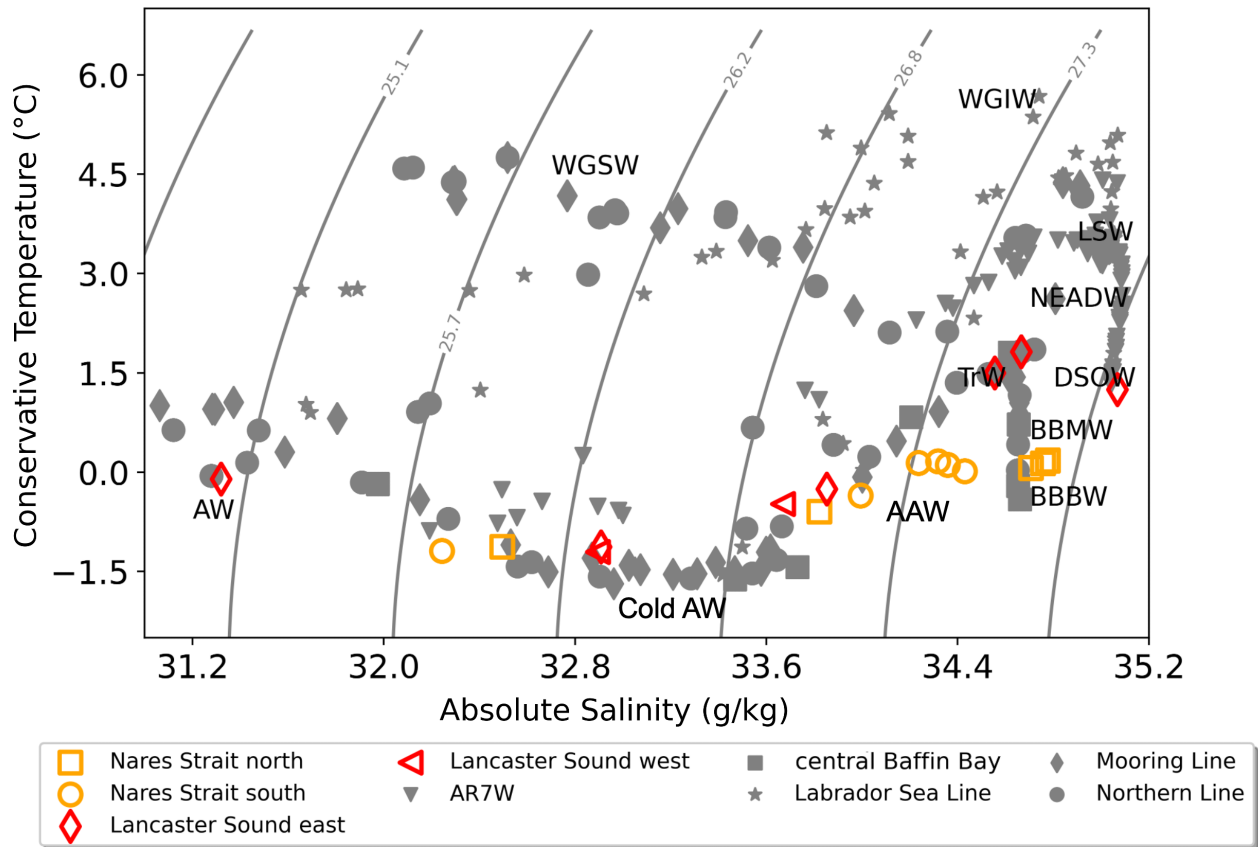


**Figure A2.** T – S diagram of all samples reported in this study. Grey symbols represent the samples covering the four lines and central Baffin Bay sampled in 2022. The red symbols represent samples from Lancaster Sound, while the orange symbols represent the samples from Nares Strait, both sampled in 2024.

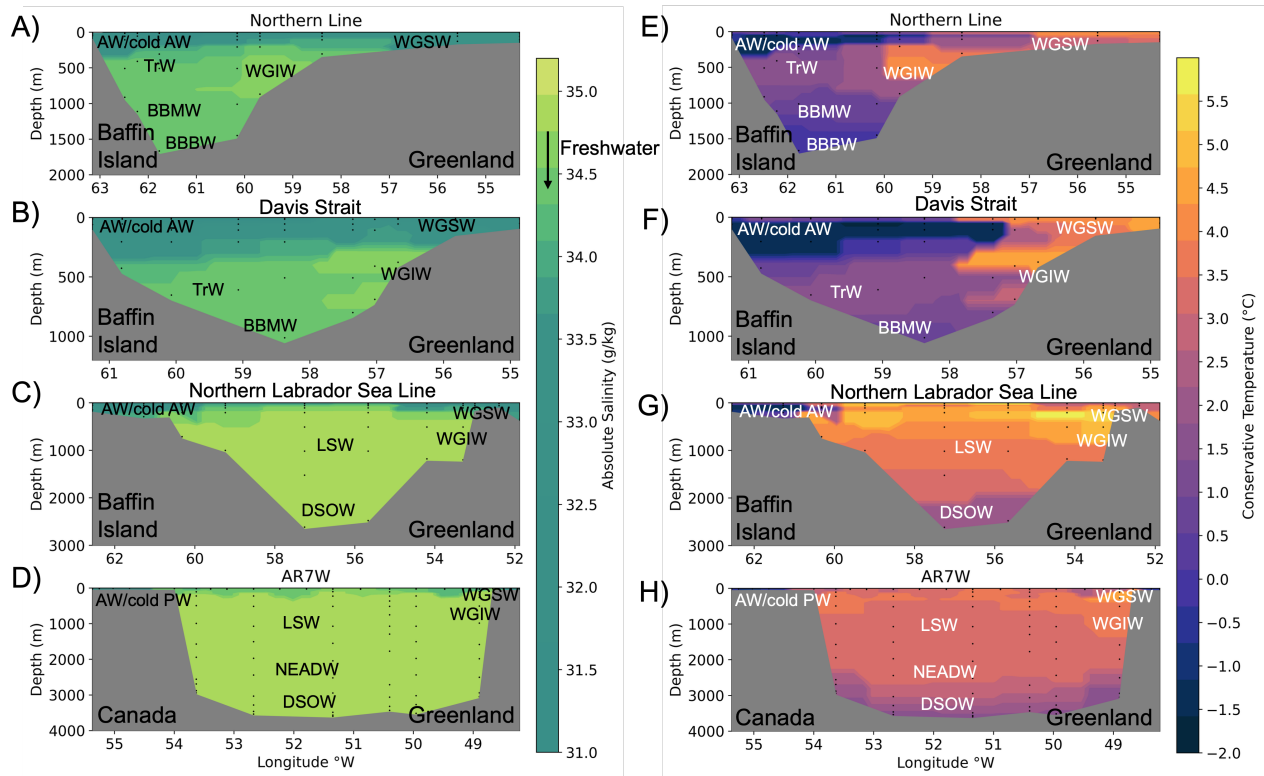


**Figure A3.** Section plots of absolute salinity (A – D) and conservative temperature (E – H), along the Northern Line (A, E), Davis Strait (B, F), Northern Labrador Sea Line (C, G), and AR7W Line (D, H).

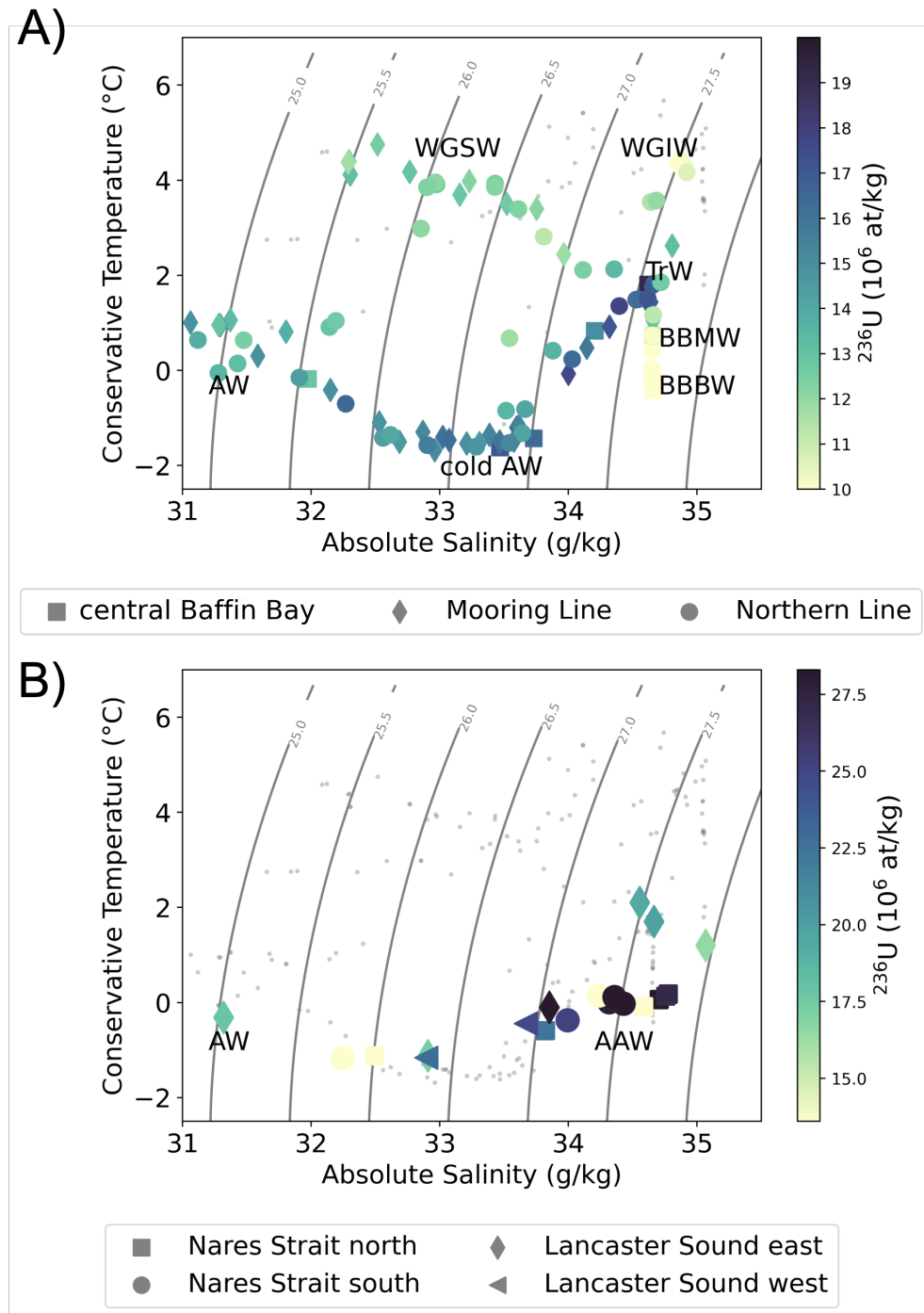


**Figure A4.** T – S diagram with colored  $^{236}\text{U}$  concentrations **A)** along Davis Strait and Northern Line, and in central Baffin Bay. **B)** The single stations at Nares Strait and Lancaster Sound. The grey dots indicate the other samples of this study.

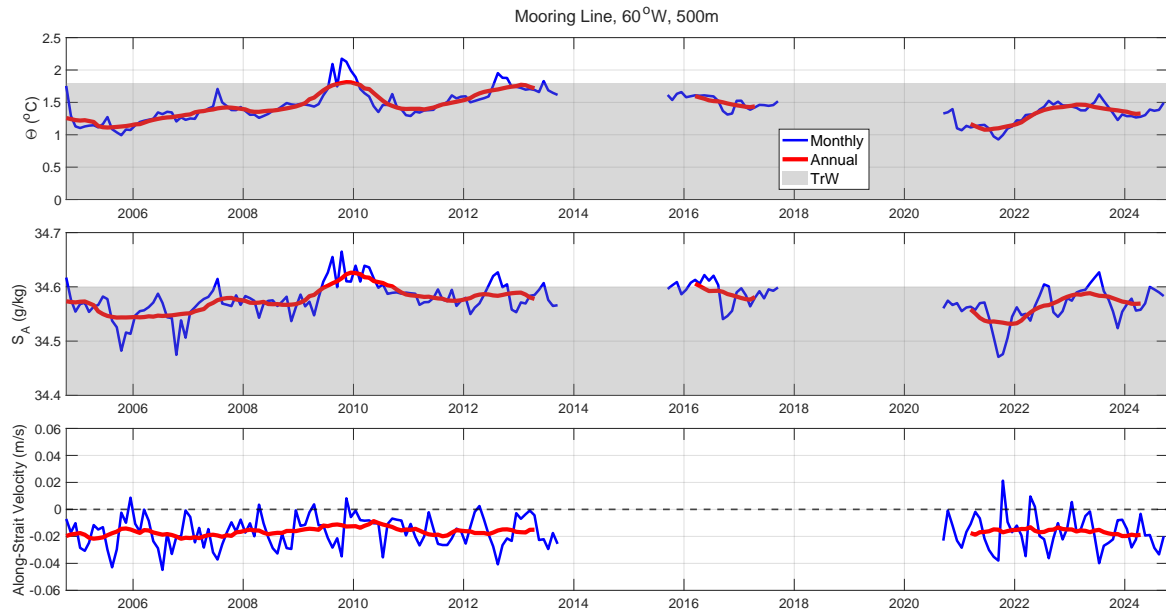


**Figure A5.** Time series of **A**) Conservative temperature ( $\Theta$ ), **B**) absolute salinity ( $S_A$ ), and **C**) along-strait velocity, at  $60^\circ\text{W}$  and 500 m depth at Davis Strait. The blue line shows the 30-day running mean and the red line shows the 12-month running mean. The  $\Theta$ - $S_A$  bounds of Transition Water are shown in grey.